ROYAL SOCIETY OF CHEMISTRY

PAPER

Check for updates

Porous helical supramolecular columns self-organized *via* the fluorophobic effect of a semifluorinated tapered dendron

Dipankar Sahoo, [ab] Mihai Peterca, [a] Mohammad R. Imam,[a] Devendra S. Maurya [a] and Virgil Percec *[a]

The self-organizable dendron **(4-3,4-3,5)12G2X** with **X = −CO$_2$CH$_3$** and **−CH$_2$OH**, an already classic dendron, facilitating the formation of a large diversity of columnar hexagonal phases including crystalline, with intracolumnar order, and liquid crystalline, and providing access for the first time to mimics of the trans-membrane protein water channel Aquaporin was semifluorinated at eight of the sp^3 hybridized carbons of its alkyl groups to provide **(4-3,4-3,5)4F8G2X**. The self-organization of **(4-3,4-3,5)4F8G2X** was analyzed by a combination of oriented fiber intermediate angle X-ray scattering, wide angle X-ray scattering, electron density maps, and reconstructed X-ray diffractograms by emplying molecular models. These experiments demonstrated that fluorophobic effect of **(4-3,4-3,5)4F8G2X** mediated mostly *via* the helical conformation of the fluorinated fragments sharper miocrosegregation of the fluorinated fragments in the most ordered states of the resulting 12$_4$ helical porous columns. These results support the original model of self-organization of dendrons and provide access to new and simpler synthetic avenues for the construction of mimics of aquaporin channels which are of great interest for cell biology and for the next generation of membranes for water separation and water purification.
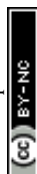
Introduction

The transmembrane protein water channel known as Aqua-porin (AQP) is one of the wonders of living cells.[1] It transports water with 100% diffusion rate and selectivity from the outer to the inner part of the cell *via* the cell membrane making our life possible. AQP consists of a helical hydrophobic pore that is responsible for this process. The first mimic of AQP was accomplished by our laboratory *via* the self-assembly of a dendritic dipeptide.[2] The stereochemistry of the dipeptide,[3] the protective groups of the dipeptide,[4] different self-assembling dendrons attached to the dipeptide,[5] the principles of self-assembly with the original dendritic dipeptide,[6,7] as well as combinations of L-Tyr with all nonpolar α-aminoacids[8] were investigated. The AQP mimic self-assembled from this dendritic dipeptide into the membrane of liposomes[9] and polymersomes[10] was demonstrated to transport water selectively. The stereochemistry of the dendritic dipeptides was used to study the role of the stereochemical information in supramolecular polymerization[11] and to self-assemble hollow

spherical supramolecular containers.[12] Dendritic dipeptides as AQP mimics pioneered a new concept for water purification that generated a new research field investigated world-wide.[13–20]

Since the early days of AQP mimics[2] in order to provide technologic accessibility we were concerned with the design of the simplest and most efficient porous helical supramolecular columns that can be homeotropically self-organized on a planar surface. The already classic original architecture, **(4-3,4-3,5)-12G2X** where X is a functional group, of the self-assembling dendron was shown to be most influential with flexible taper repeat units based on benzyl ethers,[21,22] biphenylmethyl ethers,[23] phenylpropyl ethers,[24] more complex building blocks,[25] biphenyl-propyl ethers,[26] and with the rigid *meta*-terphenyl.[27] A periodic table of self-assembling dendrons also supported this architecture as the most efficient for the construction of helical supramole-cular columns.[26,28] Indeed, helical porous supramolecular columns were ultimately self-organized in our laboratory in the absence of the dipeptide fragment of the dendritic dipeptide.[29] A cooperative and synergistically enhanced thermal stability of supramolecular columns combined with homeotropic alignment is best accomplished by semifluorination *via* the fluorophobic effect to be discussed later.[30–50] A cooperative and synergistic combination of effects could represent the key towards the technologic development of water membranes based on AQP mimics. This is because fluorination could reduce, *via* the

[a] *Roy & Diana Vagelos Laboratories, Department of Chemistry, University of Pennsylvania, Philadelphia, Pennsylvania 19104-6323, USA.*
E-mail: percec@sas.upenn.edu
[b] *Department of Medicine, Perelman School of Medicine, University of Pennsylvania, Philadelphia, Pennsylvania 19104-6323, USA*

This journal is © The Royal Society of Chemistry 2024

J. Mater. Chem. B, 2024, **12**, 12265–12281 | **12265**

fluorophobic effect, the size of the building blocks while maintaining or even increasing efficiency. Homeotropic alignment on planar surfaces is fundamental to the contruction of membranes with perfect pore alignment. In addition, fluoroethers elaborated in our laboratory,[51] facilitate both the homeotropic assembly and special effects in biological membranes.[46–49] Indeed semifluorination has been reported recently by our laboratory[52] to induce a helical porous supramolecular column from the classic perhydrogenated **(4-3,4-3,5)12G2X**, where X is –CO_2CH_3 or –CH_2OH, architecture employed in the construction of dendritic dipeptide without the attachment of the dipeptide[2] at its apex. However, the detailed supramolecular structure of this helical porous semifluorinated AQP mimic was not yet elucidated.[52] The goal of this paper is to determine the supramolecular structure of the semifluorinated helical porous assembly and elaborate its principles of self-organization.

Results and discussion

A brief introduction to fluorous chemistry and fluorous phase in self-assembly

In 1994 Horvath and Rabai advanced the concept of fluorous chemistry[53] which evolved rapidly in a new field of research.[54] Highly fluorinated sp^3 hybridized hydrocarbons are immiscible at low, including room temperature, with the homologous hydrogenated compounds forming a biphasic system. However, at high temperature they generate a homogeneous solution. This property can be exploited for homogeneous reactions at high temperature followed by simple isolation of the catalysts, starting materials and products, which are preferentially soluble in one of the two phases, at low temperature. Conventional catalysts or ligands can be conjugated to a fluorinated tail which facilitates their transplant in the fluorinated solvent at low temperature and in the homogeneous solution at high temperature. An infinite number of methodologies can be or were already elaborated based on this concept.[54] Aside from the excellent handbook of fluorous chemistry[54] numerous review articles on fluorous chemistry and in self-assembly as well as disassembly *via* fluorous chemistry are available.[55–63] The most general view is that microsegregation of the fluorinated fragments from the hydrogenated one are providing a special driving force that mediates self-assembly *via* the fluorous phase. At least in the case of columnar self-organizations a cooperative and synergistic effect of the fluorous phase as a function of the length of the perfluorinated alkyl group was observed.[30,31,64] Cooperative and synergistic effects were encountered in chemical and biological sciences including in chemical biology, catalysis, materials design, and methodology and in many cases they were elucidated.[65–71] A cooperative and synergistic effect was reported also during metal-catalyzed living radical polymerization in different mixtures of solvents.[72] However, the mechanism of this cooperative and synergistic effect continues to be under ellucidation.[72] Although this effect is not yet elucidated[72] it is hypothesized that a certain ratio between the two solvents provides a catalytic effect for the mixture of solvents employed,[73] yielding living radical polymerizations with complete

conversion and zero termination.[74] This process is demanded by the synthesis of polymers with complex architecture[75] and morphology[76,77] from conventional monomers.[75] We will elaborate more on this concept in the next subchapters.

Synthesis of (4-3,4-3,5)4F8G2X with X = CO_2CH_3 and CH_2OH

This synthesis of **(4-3,4-3,5)4F8G2X** with X = –CO_2CH_3 and –CH_2OH is based on well-established procedures elaborated previously in our laboratory[31,33,40,52] and therefore, they will be described only briefly in Scheme 1 without repeating the analytical data which were reported previously.
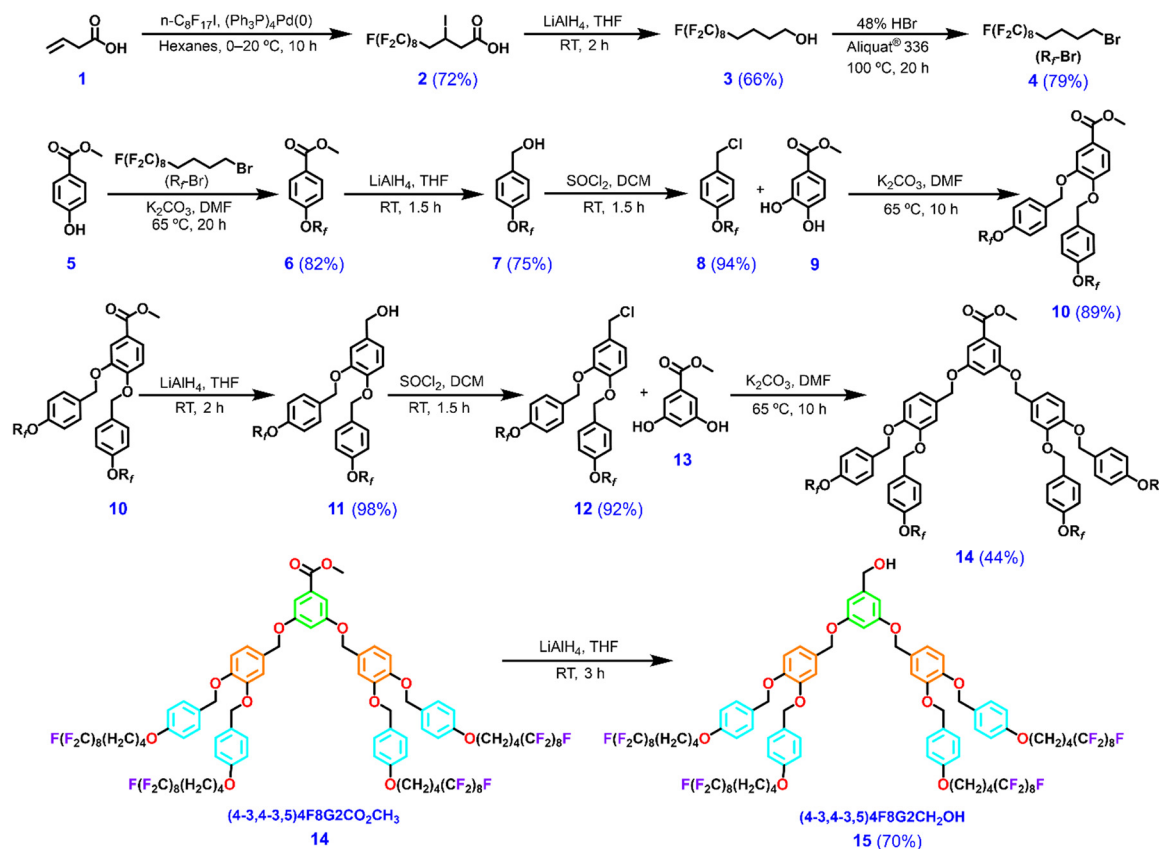
Compound **2** was synthesized by the Pd(0) catalyzed radical addition of *n*-perfluorooctyl iodide to **1**.[31,33] The acid in **2** was reduced using LiAlH₄ to afford alcohol **3**.[31,33] The bromination of alcohol **3** with 48% HBr under phase transfer catalyzed conditions with Aliquat 336 as phase transfer catalyst (PTC) gave **4**.[31,33] Methyl 4-hydroxybenzoate **5** was alkylated with semifluorinated alkyl bromides **4** in DMF with K₂CO₃ as base to obtain **6**.[31,33] The ester of **6** was reduced to the alcohol **7** using LiAlH₄ followed by chlorination of the alcohol **7** to the benzyl chloride **8** using thionyl chloride.[33,40] The dendron **10** was synthesised using methyl 3,4-dihydroxybenzoate **9** and with the benzyl chloride **8** in DMF using K₂CO₃ as base.[52] The ester of dendron **10** was reduced to the alcohol **11** using LiAlH₄ followed by chlorination of alcohol **11** to the benzyl chloride **12** using thionyl chloride.[52] Second generation dendron **14** was synthesized by etherification 3,4-dihydroxybenzoate **13** with **12** in DMF with K₂CO as base.[52] Finally the ester **14** was reduced using LiAlH₄ to the benzyl alcohol **15**. All compounds were characterized by a combination of ¹H- and ¹³C-NMR, HPLC, and MALDI-TOF to demonstrate higher purity than 99% and were reported previously.[52]

Characterization of (4-3,4-3,5)4F8G2X self-organizations by differential scanning calorimetry

Differential scanning calorimetry (DSC) experiments performed with 10 °C min⁻¹ were employed to determine phase transitions and their associated enthalpy changes for the self-organizations of **(4-3,4-3,5)4F8G2X** (Fig. 1 and Table 1). As separated from the reaction mixture **(4-3,4-3,5)4F8G2X** exists in a glassy state which self-organizes *via* an exothermic transition, which occurs immediately above the glass transition temperature, into a crystalline columnar hexagonal periodic array. This periodic array is maintained after numerous heating and cooling scans in bulk state although it changes *via* first order phase transitions from crystalline to columnar hexagonal with intracolumnar order (io) and to liquid crystalline columnar hexagonal phase. The nature of the phases associated with phase transitions determined by DSC was determined by oriented fiber X-ray diffraction experiments which will be discussed in the next subchapter.

During the first heating scan **(4-3,4-3,5)4F8G2CO₂CH₃** exhibits, just above the glass transition temperature (T_g), an exothermic crystallization which provides a columnar hexagonal crystalline periodic array denoted Φ_h^k. At 137 °C Φ_h^k melts into a columnar hexagonal phase with intracolumnar order, Φ_h^{io} which transforms into a columnar hexagonal liquid crystal state, Φ_h, undergoing

12266 | *J. Mater. Chem. B*, 2024, **12**, 12265–12281

This journal is © The Royal Society of Chemistry 2024

Scheme 1 Synthesis of **(4-3,4-3,5)4F8G2X** with **X = CO₂CH₃** and **CH₂OH**.

isotropization at 204 °C. During the cooling DSC scan the isotropic liquid forms the columnar hexagonal liquid crystal phase, Φ_h, at 201 °C. At 111 °C the liquid crystal phase, Φ_h, transforms into Φ_h^{io} which crystallizes at 96 °C. During the second
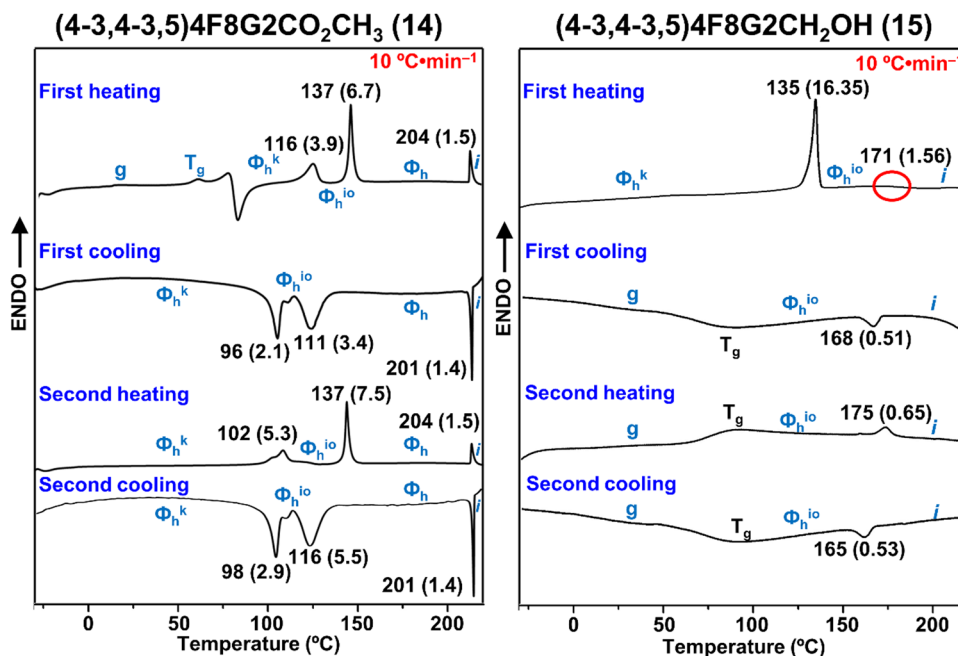

Fig. 1 DSC traces collected for **(4-3,4-3,5)4F8G2CO₂CH₃** (**14**) and **(4-3,4-3,5)4F8G2CH₂OH** (**15**) at heating and cooling rate of 10 °C min⁻¹. Phases determined by XRD, transition temperatures (in °C), and associated enthalpy changes (in between parentheses in kcal mol⁻¹) are indicated. Φ_h^k, crystalline columnar hexagonal phase; Φ_h^{io}, columnar hexagonal phase with intracolumnar order; Φ_h, liquid crystalline columnar hexagonal phase, i: isotropic phase; g: glassy phase.

This journal is © The Royal Society of Chemistry 2024

J. Mater. Chem. B, 2024, **12**, 12265–12281 | **12267**

Paper

Table 1 Thermal analysis of the supramolecular dendrimers self-assembled from **(4-3,4-3,5)4F8G2CO$_2$CH$_3$ (14)** and **(4-3,4-3,5)4F8G2CH$_2$OH (15)**

	Phase transition (°C) and corresponding enthalpy changes[a] (kcal mol^{-1})	
Compound	Heating	Cooling
(4-3,4-3,5)4F8G2CO$_2$CH$_3$	g 80 Φ_h^k 116 (3.9) Φ_h^{io} 137 (6.7) Φ_h 204 (1.5) i	i 201 (−1.4) Φ_h 111 (−3.4) Φ_h^{io} 96 (−2.1) Φ_h^k
	Φ_h^k 102 (5.3) Φ_h^{io} 137 (7.5) Φ_h 204 (1.5) i	i 201 (−1.4) Φ_h 116 (−5.5) Φ_h^{io} 98 (−2.9) Φ_h^k
(4-3,4-3,5)4F8G2CH$_2$OH	Φ_h^k 135 (16.35) Φ_h^{io} 171 (1.56) i	i 168 (−0.51) Φ_h^{io} 80 g
	g 80 Φ_h^{io} 175 (0.65) i	i 165 (−0.53) Φ_h^{io} 80 g

[a] Data from the first heating and cooling scans (at 10 °C min^{-1}) are on the first line, and data from the second heating are on the second line; Φ_h^k, crystalline columnar hexagonal phase; Φ_h^{io}, columnar hexagonal phase with intracolumnar order; Φ_h, columnar hexagonal liquid crystalline phase i: isotropic phase; g: glass phase.

heating scan we do not see the crystallizatiuon exotherm since crystallization occurs during cooling *via* the exotherm at 96 °C. However, we observe the melting transition at 102 °C which is at lower temperature than during the first heating scan. Transitions to the columnar hexagonal liquid crystal and isotropization temperatures occur at the same temperatures as during the first heating scan, *i.e.*, at 137 and 204 °C. Transitions during the second cooling scan are identical or almost identical to those of the first cooling scan. It is important to remark that isotropization on heating and cooling scans occurs with little supercooling and with identical associated enthalpies. Transitions from columnar hexagonal phase with intracolumnar order to the columnar liquid crystalline phase occur with a small degree of supercooling while crystallization during the cooling scan occur with higher decree of supercooling. These trends are expected and were explained in previous publications from our laboratory.[78,79] It is interesting to observe that the self-organized **(4-3,4-3,5)4F8G2CH$_2$OH** exhibits, during the first heating scan, a columnar hexagonal crystalline phase, Φ_h^k, which melts at 135 °C directly into a columnar hexagonal liquid crystal, Φ_h, undergoing isotropization at 171 °C. On the cooling scan the isotropic liquid transforms into the columnar hexagonal liquid crystal state at 168 °C. No crystallization was observed during the cooling scan. Most probably crystallization is kinetically prohibited by the glass transition temperature (T_g) of the supramolecular structure. Subsequent heating and cooling DSC scans show only the glass transition temperature followed by the columnar hexagonal liquid crystal, Φ_h, and its isotropization temperature. Therefore, the functional group X attached to the apex of the **(4-3,4-3,5)4F8G2X** affects quite substantially the thermal behavior of the supramolecular assembly, the ester group favoring crystallization as well as the formation of the columnar hexagonal phase with intracolumnar order, Φ_h^{io}. The alcohol group attached to the apex disfavors crystallization and formation of the Φ_h^{io} phase. It must be pointed out that the corresponding hydrogenated dendron, **(4-3,4-3,5)12G2CH$_2$OH**, exhibits a columnar hexagonal liquid crystal phase which undergoes isotropization at 132 °C, which is about 40 °C lower than of the corresponding semifluorionated periodic array.[2,6] This sensitivity of the supramolecular assembly to the functional group at the apex is in line with other examples in which the primary structure of the self-assembling dendron influences its self-organization

process,[80–82] including additional unpublished work from our laboratory which will be published soon.

Structural analysis of the self-organizations of (4-3,4-3,5) 4F8G2CO$_2$CH$_3$ by oriented fiber X-ray diffraction experiments

A combination of intermediary-angle (IAXS) and wide-angle X-ray scattering (WAXS) performed on oriented fibers together with experimental density was used to construct molecular models employing methodologies developed and used routinely in our laboratory.[82–87] Suitable molecular models, agreeing with the experimental dimensions and densities, were used to reconstruct the experimental X-ray data. This methodology was employed to provide the structural analysis of all self-organizations. Fig. 2 presents representative oriented fiber X-ray diffractograms.

Fig. 2a–f shows IAXS and WAXS recorded at different temperatures corresponding to different phases of **(4-3,4-3,5) 4F8G2CO$_2$CH$_3$** together with the lattice symmetry and lattice parameters. Oriented fiber IAXS combined with WAXS at 30 °C shown in Fig. 2a and b demonstrated the assembly of the Φ_h^k phase, at 130 °C in Fig. 2c and d, demonstrated a Φ_h^{io} periodic array, while at 160 °C in Fig. 2e and f the Φ_h liquid crystalline state. Lattice and column dimensions together with experimental densities obtained from these experiments will be employed to generate models used to reconstruct the IAXS and WAXS results from Fig. 2 and determine the structure of the supramolecular assemblies (Table 1). Fig. 2g and i show radial plots along the equatorial plane from the oriented fiber XRD pattern obtained at 130 °C in the Φ_h^{io} phase and at 160 °C in the Φ_h liquid crystal array of **(4-3,4-3,5)4F8G2CO$_2$CH$_3$** while Fig. 2f and h display the radial plots of their simulated XRD data to be discussed in Fig. 5. The very good agreement between the exterimental and simulated radial plots from Fig. 2g–j demonstrate the accuracy of the supramolecular models to be discussed later. The amplitudes of the diffraction peaks in the columnar hexagonal phase with intracolumnar order are higher than in the columnar hexagonal liquid crystal phase both in the experimental data and in the simulated results. This indicates sharper boundaries between the fluorinated and hydrogenated fragments in the columnar hexagonal array with intracolumnar order that is created most probably by an enhanced electron density contrast reflected in the more intense X-ray data collected at 130 °C. This difference supports the microsegregation

12268 | *J. Mater. Chem. B*, 2024, **12**, 12265–12281

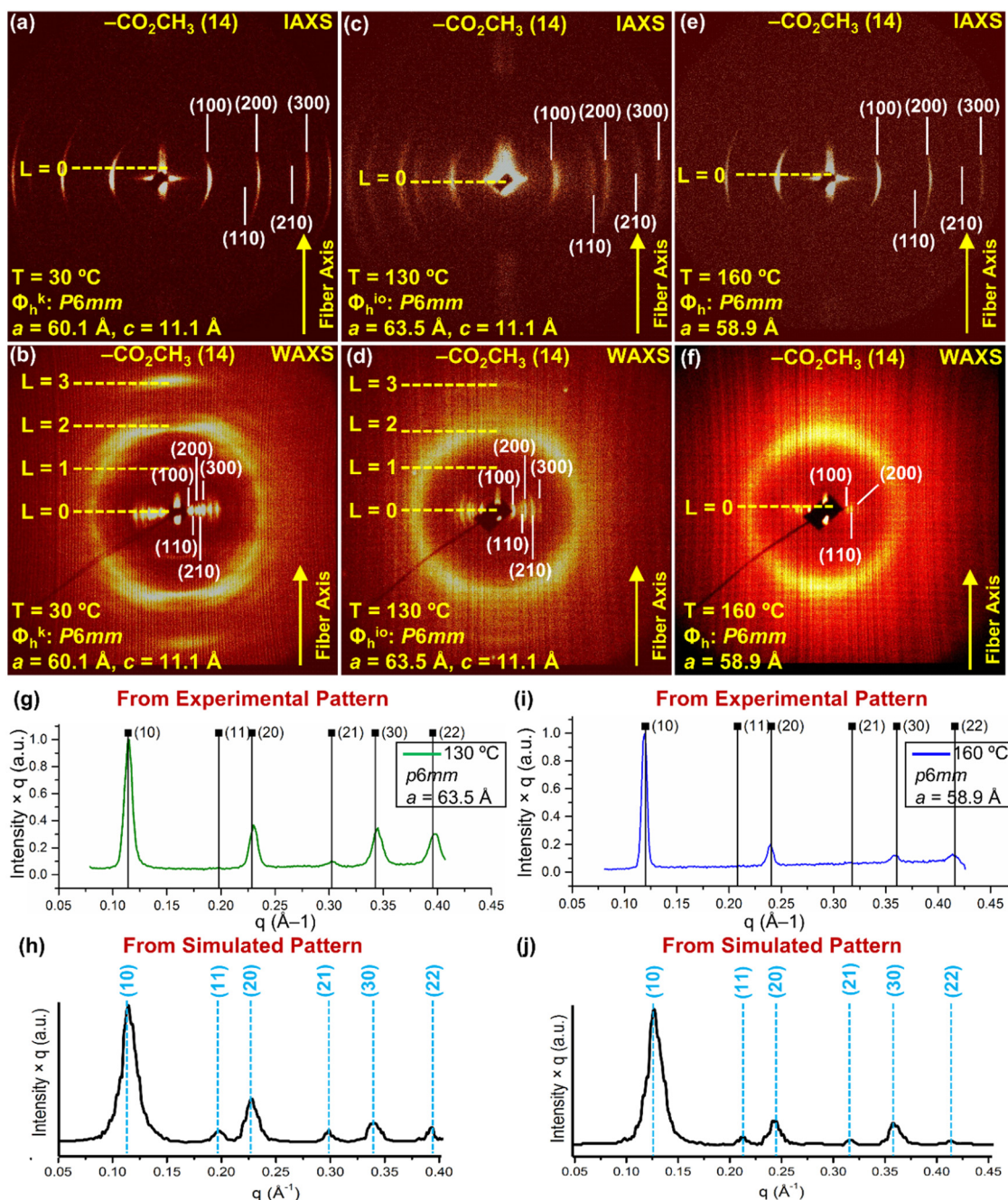This journal is © The Royal Society of Chemistry 2024

Fig. 2 Intermediate-angle oriented fiber X-ray scattering (IAXS) (a), (c) and (e) (top row) and wide-angle oriented fiber X-ray scattering (WAXS) (b), (d) and (f) (bottom row) of the self-organizations of **(4-3,4-3,5)4F8G2CO$_2$CH$_3$ (14)**. (g) Radial plot along the equatorial plane from the XRD pattern at 130 °C. (h) Radial plot of the simulated XRD pattern obtained from the molecular model to be discussed in Fig. 4. (i) Radial plot along the equatorial plane from the XRD pattern at 160 °C. (j) Radial plot of the simulated XRD pattern obtained from molecular models to be discussed in Fig. 5. The temperature at which the XRD data was measured, crystal lattice with space groups, layer lines, cell parameters, d-spacings, and the fiber axes are shown.

role of the fluorophobic effect in self-organization. We expect an even higher intensity of the diffraction peaks in the crystal states of these supramolecular assemblies.

Structural analysis of the self-rganizations of (4-3,4-3,5)-4F8G2CH$_2$OH by oriented fiber X-ray diffraction experiments

Fig. 3 provides examples of oriented fiber IAXS and WAXS at different temperatures in the Φ_h^k phase and in the Φ_h liquid crystal state of the periodic arrays self-organized from **(4-3,4-3,5)4F8G2CH$_2$OH**. The combination of oriented fiber IAXS and WAXS recorded at 100 °C (Fig. 3a and b) demonstrates a columnar hexagonal crystalline self-organization Φ_h^k, while at 160 °C a columnar hexagonal liquid crystal phase Φ_h. Lattice dimensions are indicated on the diffractograms and will be used to construct the molecular models employed to reconstruct the experimental X-ray diffractograms. Fig. 3e and g show
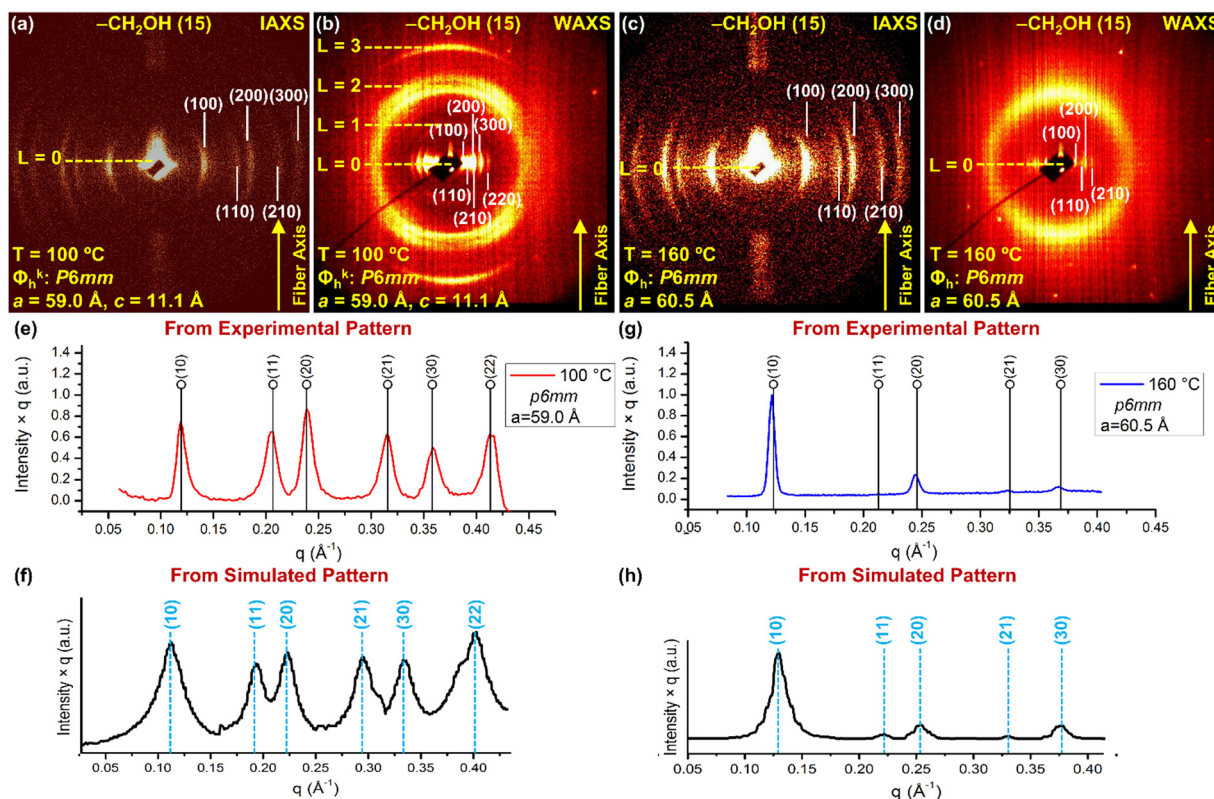
This journal is © The Royal Society of Chemistry 2024

J. Mater. Chem. B, 2024, **12**, 12265–12281 | **12269**

Fig. 3 (a) Intermediate-angle oriented fiber X-ray scattering (IAXS) (a) and (c) and wide-angle oriented fiber X-ray scattering (WAXS) (b) and (d) of (**4-3,4-3,5)4F8G2CH₂OH** (**15**). (e) Radial plot along the equatorial plane from the XRD pattern at 100 °C. (f) Radial plot of the simulated XRD pattern obtained from the molecular model to be discussed in Fig. 6. (g) Radial plot along the equatorial plane from the XRD pattern at 160 °C. (h) Radial plot obtained from the simulated pattern obtained from the supramolecular model to be discussed in Fig. 7. The temperature at which the XRD data was measured, crystal lattice with space groups, layer lines, cell parameters, *d*-spacings, and the fiber axes are shown.

the radial plots along the equatorial plane from the XRD data at 100 °C in the Φ_h^k phase while Fig. 3g shows the radial plots along the equatorial plane from the XRD data at 160 °C in the Φ_h liquid crystalline state. The enhanced amplitudes of the diffractograms from Fig. 3e are higher than the one from Fig. 3f supporting a better microsegregation of the fluorinated fragments in the crystal state than in the liquid crystal state. The intensities of the radial plots of the experimental XRD data from Fig. 3e and f agree with the radial plots obtained from the simulated XRD results (Fig. 3f and h) demonstrating that the supramolecular models employed to simulate these diffraction data and to be discussed later are correct. It is also very important to remark here that the intensities in the columnar hexagonal crystalline phase (Fig. 3e) are higher than in the columnar hexagonal phase with intracolumnar order (Fig. 2g).

To our knowledge, this may be the first report demonstrating the role of the fluorophobic effect in self-organization. Therefore, we must point out the main difference between perhydrogenated and perfluorinated sp³ hybridized compounds. Perfluorinated carbon chains adopt a helical conformation induced by the electrostatic repulsion of fluorine atoms in the 1,3-positions of the crystal state and in solution while linear perhydrogenated hydrocarbons display a zig-zag conformation. The helical conformation of perfluorinated carbon chains was first demonstrated by Bunn and Howells in TEFLON

by X-ray diffraction experiments.[88] This helical conformation was shown in shorted perfluorinated alkyl chains such as octyl both in solid state as well as in solution by a combination of theoretical calculations combined with ¹⁹F-NMR and vibrational circular dichroism.[89,90] We must state that the helical conformation of the fluorinated alkyl groups both in ordered states and in solution was neglected previously when the fluorophobic effect was employed to explain the mechanism of self-organization. Since perfluorinated alkanes cannot adopt any other conformation but helical,[88–90] we strongly suggest that the helical conformation of the perfluorooctyl fragments of (**4-3,4-3,5)4F8G2CH₂X** is responsible for the most efficient fluorophobic effect in ordered states. This concept will be discussed in more details with 3-dimensional (3D) molecular models.

Dimensions of supramolecular assemblies determined by XRD experiments together with experimental densities (Table 2) were employed to construct and screen 3D molecular models of the supramolecular columns self-organized from (**4-3,4-3,5)4F8G2X**. These models were used to reconstruct the oriented fiber X-ray diffractograms by methods employed routinely in our laboratory.[83–87] Agreement between the experimental and reconstructed X-ray results was used to decide that the model was suitable for the structure analyzed as briefly mentioned in Fig. 2 and 3 (Table 2). Fig. 4 shows the analysis of the columnar hexagonal crystalline columns self-organized from

12270 | *J. Mater. Chem. B*, 2024, **12**, 12265–12281

This journal is © The Royal Society of Chemistry 2024

Table 2 Structural analyses of **(4-3,4-3,5)4F8G2CO$_2$CH$_3$ (14)** and **(4-3,4-3,5)4F8G2CH$_2$OH (15)** by XRD

	T (°C)	Phase[a]	a^b (Å)	ρ^c (g cm^{-3})	M_{wt}^d (g mol^{-1})	t^e (Å)	μ^f	D_{col}^g (Å)	$d_{10}, d_{11}, d_{20}, d_{21}, d_{30}, d_{22}^h$ (Å)
14	30	Φ_h^k	62.7	1.58	2733.53	3.7	4	62.7	54.7, 31.5, 27.2, 20.6, 18.2, 15.7
	130	Φ_h^{io}	63.5			3.7	4	63.5	55.1, 32.0, 27.3, 20.7, 18.2, 15.8
	170	Φ_h	61.1			—	4	61.1	53.3, 30.6, 26.5, 20.0, —, —
15	100	Φ_h^k	59.0	1.58	2705.52	—	4	59.0	51.3, 29.6, 25.6, 19.3, 17.0, 14.8
	160	Φ_h^{io}	60.5			3.7	4	60.5	52.7, 30.3, 26.2, 19.9, 17.5, —

[a] Φ_h^{io}, liquid crystalline columnar hexagonal phase; Φ_h^k, crystalline columnar hexagonal phase. [b] Lattice parameters (with uncertainty of ~1%) calculated $a = (2/\sqrt{3})(d_{100} + \sqrt{3}d_{110} + 2d_{200})/3$ for the Φ_h phase. [c] Experimental density (ρ) measured at room temperature (24 °C). [d] Molecular weight (M_{wt}) of the compound. [e] Stratum thickness calculated from the WAXS pattern. [f] Average number of molecules in the unit cell, calculated using $\mu = N_A A t \rho / M_{wt}$ where $N_A = 6.022 \times 10^{23}$ mol^{-1} = Avogadro's number, A is the area of the column cross-section calculated from the lattice parameters and ρ is the density. [g] Column diameter for Φ_h phase calculated using $D_{col} = a$. [h] Experimental diffraction peaks d-spacings for Φ_h phase calculated using $d_{hk} = (\sqrt{3}a/2)(h^2 + k^2 + hk)^{-1/2}$.

(4-3,4-3,5)4F8G2CO$_2$CH$_3$. Fig. 4a shows the experimental and reconstructed X-ray of the columnar hexagonal crystalline periodic array assembled from the supramolecular column illustrated in Fig. 4b–e which shows the side view of the crown conformation of column cross-section assembled from 4 dendrons, the top view of the first layer of the column, the top view
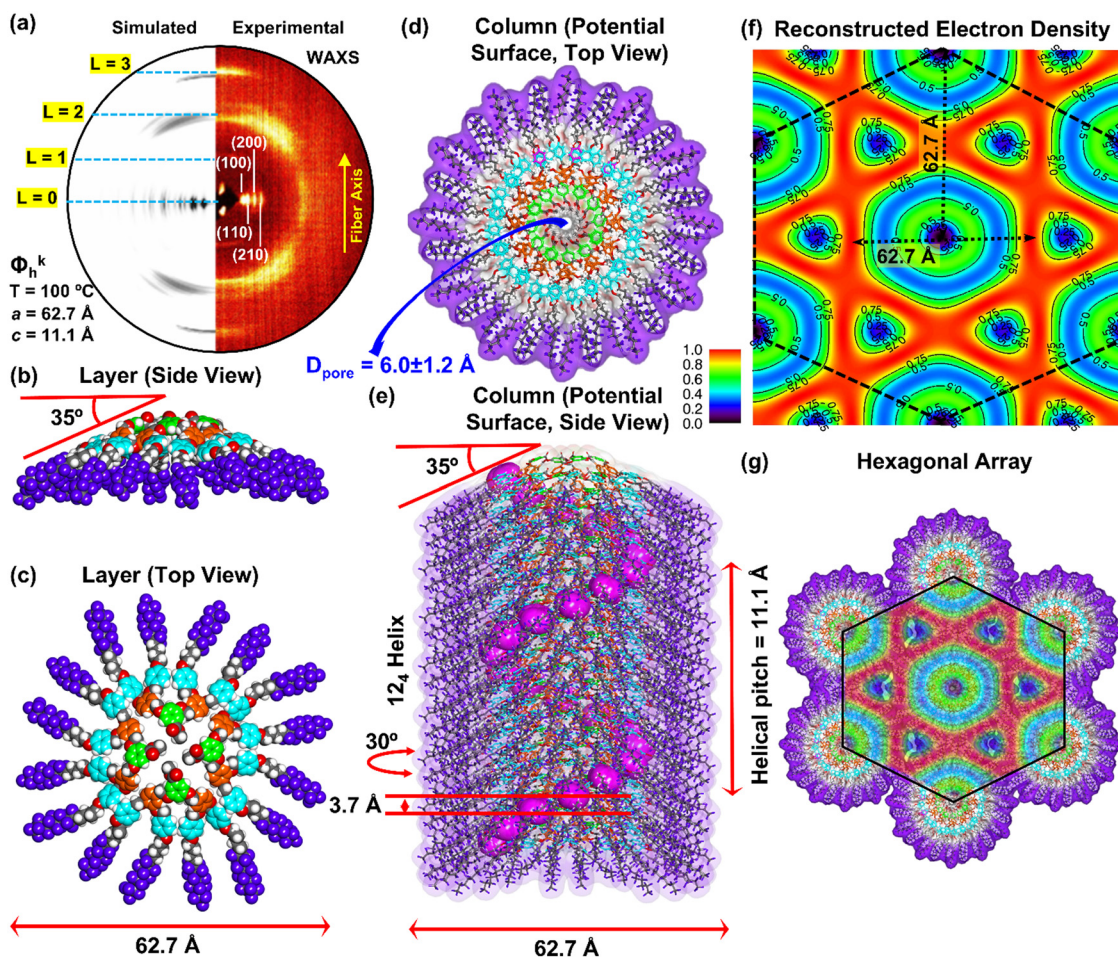

Fig. 4 X-ray diffraction analysis and molecular models of at 100 °C (Φ_h^k phase). (a) Wide-angle fiber XRD patterns (WAXS) and simulated XRD patterns from the molecular model showing the similarity; (b) formation of the layer by four molecules showing the tilt angle (side view); (c) layer with four molecules (top view); (d) formation of the column by repeat of the tetramer layer (potential surface, side view); (e) column (potential surface, top view); (f) reconstructed relative electron density map; (g) hexagonal array by the columns (potential surface; top view). Color codes used in the molecular models are similar as shown in the ChemDraw structure of **14**. O atoms, red; H atoms, white; F atoms, purple; C atoms in the phenyl rings connected apex −CO$_2$CH$_3$ group, green; C atoms in the phenyl rings connected of the first generation, orange; C atoms in other phenyl rings in the second generation, light blue; all other C atoms, grey. Potential surface is in fact the "van der Waals surface" and the color codes for the potential surface are similar as the colors of the atoms; transparency (50%) was added for clarity.

of the entire column and the entire column respectively. The reconstructed electron density map generated from the experimental X-ray diffractogram is shown in Fig. 4f. Fig. 4g illustrates the columnar hexagonal array generated from the supramolecular columns from Fig. 4e together with the reconstructed electron density from Fig. 4f overlapped on top of it. All these data demonstrate that the helical porous supramolecular column from Fig. 4e represents a suitable model for the self-organized structure generated from **(4-3,4-3,5)4F8G2CO$_2$CH$_3$**.

The architectures of (4-3,4-3,5)4F8G2CO$_2$CH$_3$ self-organizations

Fig. 5 provides the oriented fiber experimental and reconstructed X-ray patterns in part a. The simulation was accomplished with the 3D model from Fig. 5b–f. The supramolecular column responsible for the formation of the liquid crystal state is less perfect than the one forming the crystal state. This can be seen by comparing supramolecular columns from Fig. 4e and 5f. Fig. 5g shows the reconstructed electron density obtained from experimental X-ray

results while Fig. 5h provides the hexagonal periodic array constructed from the supramolecular column of Fig. 5f. Overlap of the electron density map from Fig. 5g over the hexagonal periodic array generated from the supramolecular columns from Fig. 5f is shown in Fig. 5h. Very good agreement is observed in this figure. It is very important to compare the electron density from Fig. 4f with the electron density of Fig. 5g. Sharper boundaries of various electron densities are observed in the case of the crystalline columns from Fig. 4f when compared with the electron density of the liquid crystalline columns from Fig. 5h. This comparison supports the data shown in Fig. 2g–j which indicate higher amplitude of the diffraction peaks in higher ordered phases both in the case of the experimental and simulated XRD data.

The architectures of (4-3,4-3,5)4F8G2CH$_2$OH self-organizations

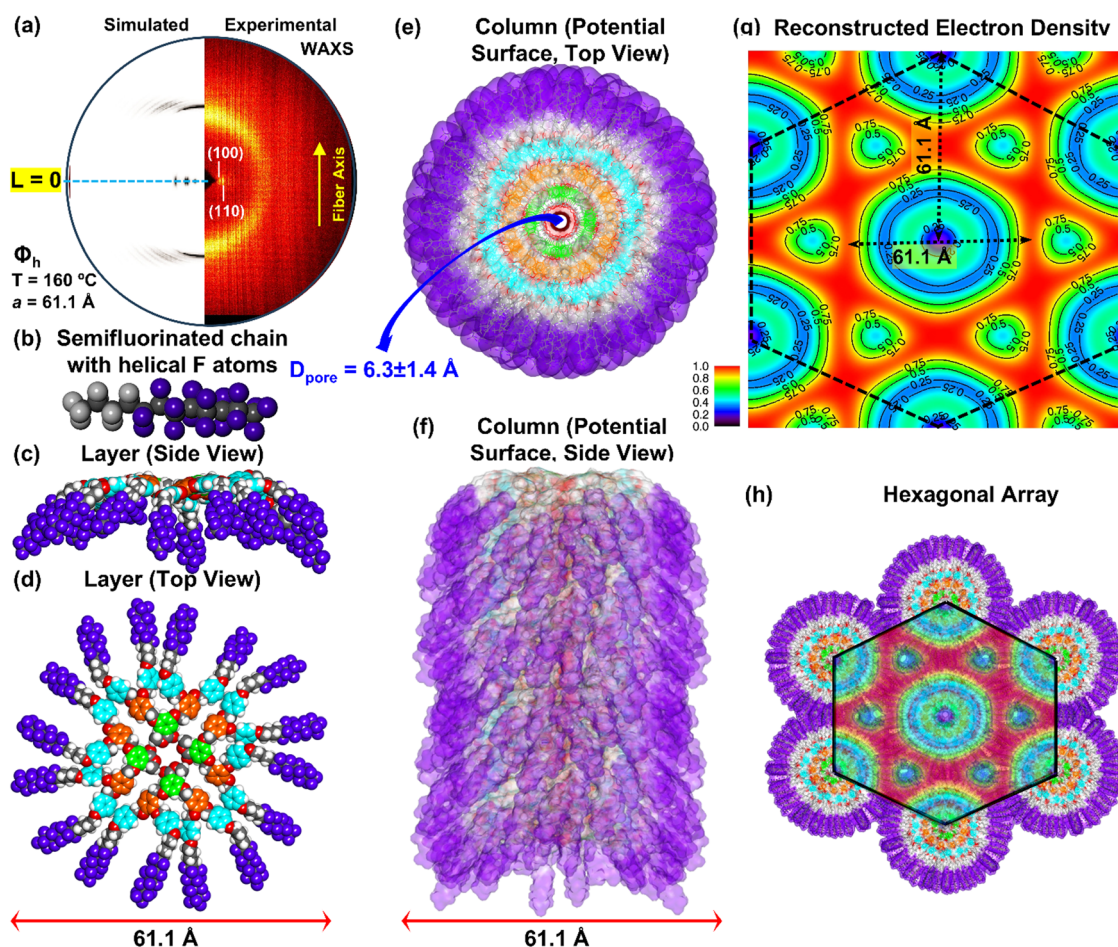Fig. 6 shows the data for the supramolecular column of **(4-3,4-3,5)4F8G2CH$_2$OH**.

Fig. 5 X-ray diffraction analysis and molecular models of **(4-3,4-3,5)4F8G2CO$_2$CH$_3$ (14)** at 160 °C (Φ_h phase). (a) Orinted fiber wide-angle XRD patterns (WAXS) and simulated XRD patterns from the molecular model showing the similarity; (b) semifluorinated chain showing the helical F atoms; (c) formation of the layer by four molecules (side view); (d) layer with four molecules (top view); (e) formation of the column by repeat of the tetramer layer (potential surface, side view); (f) column (potential surface, top view); (g) reconstructed relative electron density map; (h) hexagonal array by the columns (potential surface; top view). Color codes used in the molecular models are similar as shown in the ChemDraw structure of **14**. O atoms, red; H atoms, white; F atoms, purple; C atoms in the phenyl rings connected apex −CO$_2$CH$_3$ group, green; C atoms in the phenyl rings connected of the first generation, orange; C atoms in other phenyl rings in the second generation, light blue; all other C atoms, grey. Potential surface is in fact the "van der Waals surface" and the color codes for the potential surface are similar as the colors of atoms; transparency (50%) was added for clarity.

12272 | *J. Mater. Chem. B*, 2024, **12**, 12265–12281

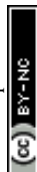This journal is © The Royal Society of Chemistry 2024

Fig. 6a displays the experimental and reconstructed fiber X-ray diffractograms. The side view of the cross-cection of the supramolecular column is in Fig. 6b. The top view of the side view from Fig. 6b is shown in Fig. 6c. The top view of the supramolecular column is in Fig. 6d while the entire column is in Fig. 6e.

The reconstructed electron density of experimental X-ray diffractogram of (4-3,4-3,5)4F8G2CH$_2$OH is in the top of Fig. 6f with the electron density for the hydrogenated structure (4-3,4-3,5)6G2CH$_2$OH is in the bottom part of Fig. 6f. The reconstructed electron density maps of the semifluorinated (4-3,4-3,5)4F8G2CH$_2$OH (Fig. 6f, top) and of the hydrogenated (4-3,4-3,5)6G2CH$_2$OH (Fig. 6f bottom) display a large difference between fluorinated and nonfluorinated structures which is best observed by the sharpness of microsegregation seen in the case of the fluorinated structure. The hexagonal periodic array constructed from the

supramolecular column from Fig. 6e is shown in Fig. 6g together with the overlap of the electron density from top of Fig. 6f. Good agreement between all these data s including the radial plots from Fig. 2 and 3 support the 12$_4$ helical porous column architecture shown in Fig. 6e. The 3D supramolecular column assembled from (4-3,4-3,5)4F8G2CH$_2$OH in the columnar hexagonal liquid crystalline state is shown in Fig. 7. Experimental and reconstructed X-ray diffractograms are in Fig. 7a. Details of the supramolecular column are shown in Fig. 7b–f. The reconstructed electron density is in Fig. 7g while the periodic hexagonal array constructed from the column of Fig. 7f is in Fig. 7h which also contains an overlapped electron density of Fig. 7g. Sharper electron density boundaries are observed in Fig. 6f rather than in Fig. 7f. This is in agreement with the higher amplitude of the diffractograms from Fig. 3e rather than Fig. 3f. Therefore, higher order of the
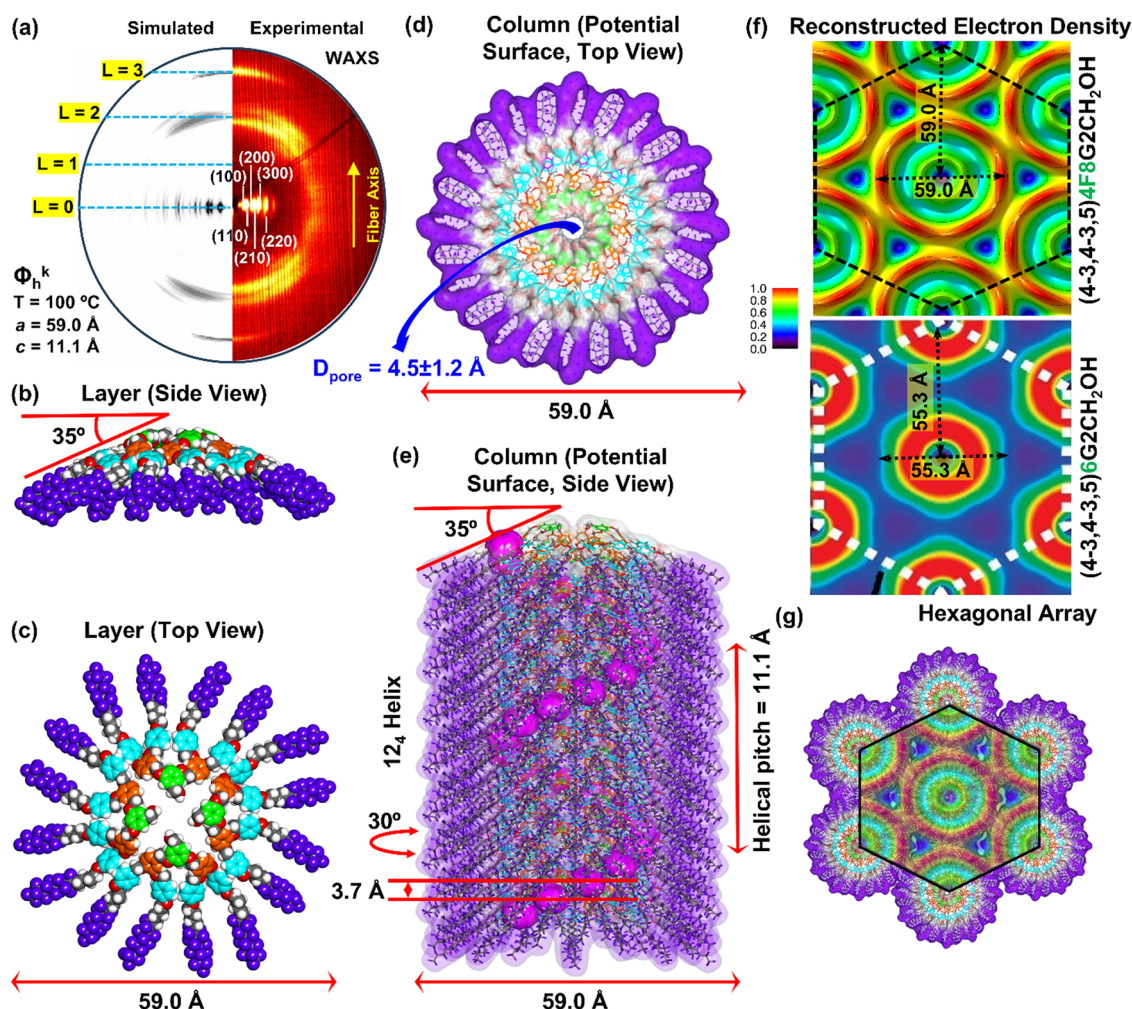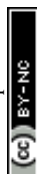

Fig. 6 X-ray diffraction analysis and molecular models of (4-3,4-3,5)4F8G2CH$_2$OH (15) at 100 °C (Φ_h^k phase). (a) Wide-angle oriented fiber XRD patterns (WAXS) and simulated XRD patterns from the molecular model showing the similarity; (b) formation of the layer by four molecules showing the tilt angle (side view); (c) layer with four molecules (top view); (d) formation of the column by repeat of the tetramer layer (potential surface, side view); (e) column (potential surface, top view); (f) reconstructed relative electron density maps of the semifluorinated (4-3,4-3,5)4F8G2CH$_2$OH (15) (top) and of the hydrogenated (4-3,4-3,5)6G2CH$_2$OH (bottom) demonstrating the large difference between fluorinated and nonfluorinated as seen in the sharpness of microsegregation observed in the case of fluorinated chains; (g) hexagonal array by the columns (potential surface; top view). Color codes used in the molecular models are similar as shown in the ChemDraw structure of 15. O atoms, red; H atoms, white; F atoms, purple; C atoms in the phenyl rings connected apex −CH$_2$OH group, green; C atoms in the phenyl rings connected of the first generation, orange; C atoms in other phenyl rings in the second generation, light blue; all other C atoms, grey. Potential surface is in fact the "van der Waals surface" and the color codes for the potential surface are similar as atom colors; transparency (50%) was added for clarity.
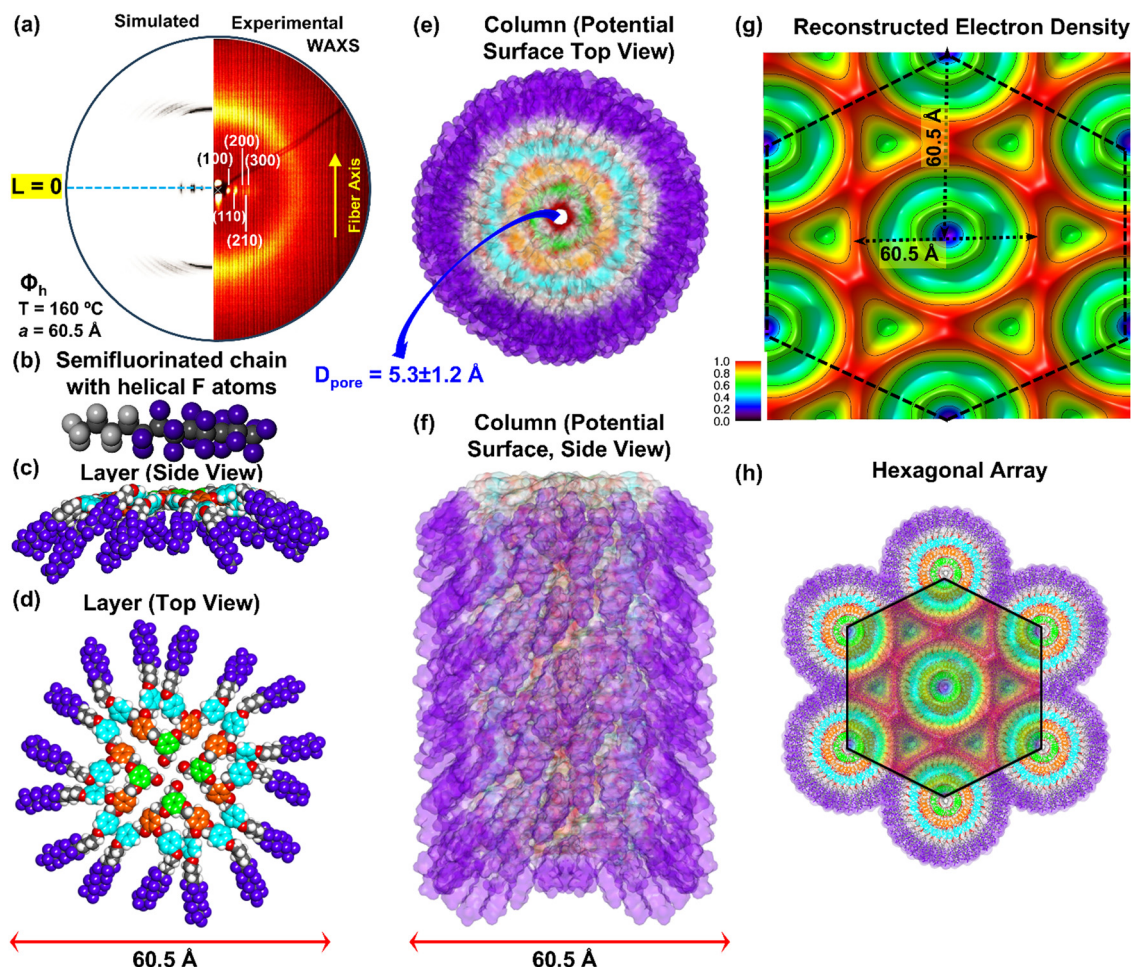
Fig. 7 X-ray diffraction analysis and molecular models of **(4-3,4-3,5)4F8G2CH₂OH** (**14**) at 160 °C (Φ_h phase). (a) Wide-angle oriented fiber XRD patterns (WAXS) and simulated XRD patterns from the molecular model showing the similarity; (b) semifluorinated chain showing the helical F atoms; (c) formation of the layer by four molecules (side view); (d) layer with four molecules (top view); (e) formation of the column by repeat of the tetramer layer (potential surface, side view); (f) column (potential surface, top view); (g) reconstructed relative electron density map; (h) hexagonal array by the columns (potential surface; top view). Color codes used in the molecular models are similar as shown in the ChemDraw structure of **15**. O atoms, red; H atoms, white; F atoms, purple; C atoms in the phenyl rings connected apex −CH₂OH group, green; C atoms in the phenyl rings connected of the first generation, orange; C atoms in other phenyl rings in the second generation, light blue; all other C atoms, grey. Potential surface is in fact the "van der Waals surface" and the color codes for the potential surface are similar to the colors, of atoms; transparency (50%) was added for clarity.

supramolecular assembly favor higher level of microsegregation and larger amplitude to the diffraction peaks observed in the radial plots from Fig. 2 and 3.

We cannot conclude before showing representative thermal optical polarized microscopy images generated by the supramolecular self-organizations of **(4-3,4-3,5)4F8G2CO₂CH₃** (**14**) and of **(4-3,4-3,5)4F8G2CH₂OH** (**15**). They are illustrated in Fig. 8. These micrographs exhibit classic focal conic textures typical for columnar hexagonal liquid crystalline phases. No attempts were made to generate homeotropic alignments. However, the textures observed at 130 °C and 200 °C indicate that they are possible.

Conclusions

The 12₄ helical porous 3D architectures self-organized from **(4-3,4-3,5)4F8G2CO₂CH₃** and **(4-3,4-3,5)4F8G2CH₂OH** were determined by a combination of oriented fiber IAXS and SAXS combined with

electron density maps and reconstruction of the experimental X-ray data with molecular models. In spite of having different functional groups at the apex, both building blocks provide helical 12₄ porous columns in their columnar hexagonal crystalline periodic arrays. This demonstrates that the fluorophobic effect provides the key role during their self-organization even if they exhibit phase transitions at different temperatures. The fluorophobic effect is more dominant in the crystalline rather than in liquid crystalline states. This is supported by both the higher amplitudes of their diffraction peaks in their X-ray diffractograms and by their reconstructed electron densities including a radial comparison with nonfluorinated structures. These data indicate that the fluorophobic effect is most probably mediated by the helical conformation of the fluorinated fragments, a factor that was not considered before this report, although the helical conformation of the flurinated alkyl groups was well established both in solid ordered state and in solution.[88–90] The ability to construct homeotropically aligned
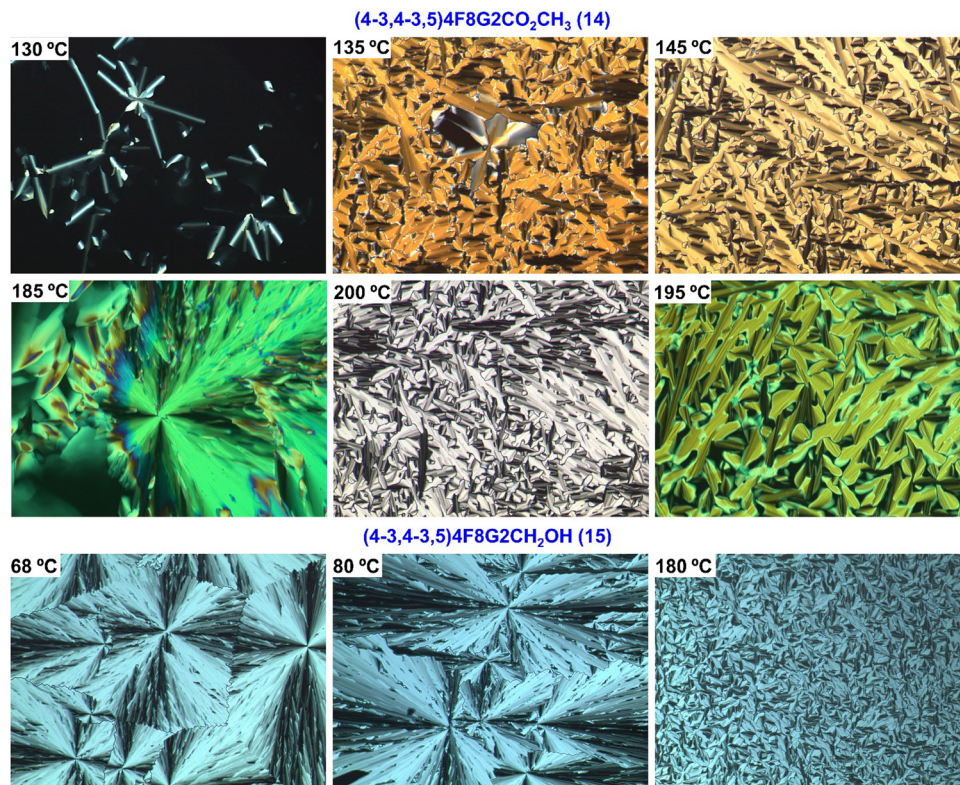
12274 | *J. Mater. Chem. B*, 2024, **12**, 12265–12281

This journal is © The Royal Society of Chemistry 2024

Fig. 8 Optical polarized microscopy images of **(4-3,4-3,5)4F8G2CO₂CH₃ (14)** and **(4-3,4-3,5)4F8G2CH₂OH (15)** at various temperatures.

supramolecular columns[33,34,91,92] together with the molecular engineering of the structure of their pore are expected to provide not only unlimited advanced in mimics of AQP but also to facilitate access to a new generation of membranes for water separation and purification.[12–20,93–100] All these features can be accomplished by combining fluorophobic effect with helical self-organization. A step towards the design of this goal was made by the research reported here. Recent progress on the synthesis of fluorinated α-aminoacids[101,102] combined with the fluorophobic effect reported here will further improve the water separation by employing simpler dendritic dipeptide structures. The enhanced microsegregation facilitated by the fluorophobic effect demonstrated here supports the original model of miscrosegregation advanced for hydrogenated building blocks.[103,104] Last but not least we believe that the role and the mechanisms of the fluorophobic effect in self-assembly,[30,32,33,35,36,39–44,50,51] in living radical polymerizations of fluorinated monomers, in fluorinated solvents, with fluorinated chain ends,[105–115] and in all other self-organization processes,[116–119] could be reevaluated and upgraded since the unlimited capabilities of the fluorinated fragments to induce helical homochirality both in self-organizations in bulk state and in solution are theoretically immense and were not yet investigated at all.
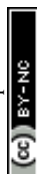
Materials and methods

Materials

Vinylacetic acid (**1**) (97%, Aldrich), perfluorooctyl iodide (99%, Fluka), LiAlH₄ (95%, Aldrich), 48% HBr (ACS reagent, Aldrich),

tricaprylylmethylammonium chloride (Aliquat 336, Aldrich), methyl 4-hydroxybenzoate (99%, Aldrich), thionyl chloride (99%, Aldrich), 3,5-dihydroxybenzoic acid (Acros, 97%), 1,1,2-trichlorotrifluoroethane (Freon 113, Acros/Fisher) were used as received. The syntheses of tetrakis(triphenylphosphine)-palladium(0) [(Ph₃P)₄Pd(0)] was performed as described previously.[96] 4-Dimethylformamide (DMF) was dried over CaH₂, filtered, and distilled under vacuum. Hexanes (ACS reagent, Fisher Scientific) used for the Pd(0) catalyzed coupling of perfluoroalkyl iodides and olefins was washed three times with concentrated H₂SO₄, three times with H₂O, and dried over anhydrous MgSO₄ before use. CH₂Cl₂ and toluene (Fisher, ACS reagent grade) were refluxed over CaH₂ and freshly distilled before use. Tetrahydrofuran (THF, Fisher, ACS reagent grade) and diethyl ether (Et₂O, Fisher, ACS reagent grade) were refluxed over sodium/benzophenone until the solution turned purple and freshly distilled before use. All other chemicals were commercially available and were used as received.

Method and techniques

The purity and structure of intermediate compounds and final products were determined by a combination of techniques including thin-layer chromatography (TLC), ¹H, ¹³C NMR, ¹⁹F NMR, high-pressure liquid chromatography (HPLC), and matrix assisted laser desorption ionization-time of flight (MALDI-TOF).

This journal is © The Royal Society of Chemistry 2024

J. Mater. Chem. B, 2024, **12**, 12265–12281 | **12275**

Thin layer chromatography (TLC)

TLC was carried out on precoated aluminum plates (silica gel with F254 indicator; layer thickness, 200 μm; particle size, 2–25 μm; pore size, 60 Å, from Sigma-Aldrich).

High pressure liquid chromatography (HPLC)

High pressure liquid chromatography (HPLC) using Shimadzu LC-20AD high-performance liquid chromatograph pump, a PE Nelson Analytical 900 Series integration data station, a Shimadzu SPD-10A VP (UV-vis, $\lambda = 254$ nm), Shimadzu RID-10A refractive index (RI) and three AM gel columns (a guard column, two 500 Å, 10 μm columns). THF was used as the solvent and the characterization was carried out at 23 °C.

Solution NMR

^{1}H NMR (400 MHz), and ^{13}C NMR (101 MHz) spectra were measured on a Bruker NEO 400 instrument using the solvent indicated.

Differential scanning calorimetry (DSC)

Thermal transitions were measured on TA instrument 2920 modulated, and Q 100 differential scanning calorimeter (DSC) integrated with a TA instrument refrigerated cooling system. The heating, and cooling rates were 10 °C min^{-1}. The transition temperatures were measured as the maxima, and minima of their endothermic, and exothermic peaks. Indium was used as the standard for the calibration.

Optical polarized microscopy

An Olympus BX-51 optical polarized microscope (40× magnification) equipped with a Metler Toldeo FP82HT hot stage, and Metler Toledo FP90 central processor was used to verify thermal transitions, and to characterize anisotropic textures.

Matrix-assisted laser desorption/ionization time of flight (MALDI-TOF)

The molar mass of all molecules was determined by MALDI-TOF mass spectrometry employing a PerSeptive Biosystem-Voyager-DE (Framingham, MA) mass spectrometer equipped with nitrogen laser (337 nm) and operating in linear mode. Angiotensin II and Bombesin were used as standards for calibration. For the preparation of sample solution, the corresponding compound was first dissolved in THF (5–10 mg mL^{-1}). Subsequently, the matrix (2,5-dihydroxybenzoic acid) was dissolved in THF 10 mg mL^{-1} and the two solutions were mixed with a 1/5 (v/v, compound solution/matrix solution) ratio. Then one drop of solution was placed on the MALDI plate and dried at 23 °C. Afterwards, the plate was inserted into the vacuum chamber of the instrument for analysis. The laser intensity and voltages applied for the analysis were adjusted based on the molar mass and nature of each compound.

Density measurements

For density measurements, a small mass of sample (0.3–0.5 mg) was placed in a vial filled with water followed by degasssed to remove the air bubbles adsorbed outside the sample. The sample sank to the bottom of the vial due to its high density compared with water. A saturated aqueous solution of potassium iodide (KI) was then added into the solution at ~0.2 g per aliquot to gradually increase the solution density. KI was added at an interval of at least 20 min to ensure equilibrium within the solution. When the sample was suspended in the middle of the solution, the density of the sample was the same as the solution, which was measured by a 5 mL volumetric flask.

X-ray diffraction (XRD)

X-ray diffraction (XRD) measurements were performed using Cu-K$_{\alpha 1}$ radiation ($\lambda = 1.542$ Å) from a Bruker-Nonius FR-591 rotating anode X-ray source equipped with a 0.2 × 0.2 mm^2 filament and operated at 3.4 kW. Osmic Max-Flux optics, and triple pinhole collimation were used to obtain a highly collimated beam with a 0.3 × 0.3 mm^2 spot on a Bruker-AXS Hi-Star multiwire area detector. To minimize attenuation and background scattering, an integral vacuum was maintained along the length of the flight tube, and within the sample chamber. Samples were held in glass capillaries (1.0 mm in diameter), mounted in a temperature-controlled oven (temperature precision: ±0.1 °C, temperature range from −10 °C to 210 °C). Aligned samples for fiber XRD experiments were prepared using a custom-made extrusion device.[83–87] The powdered sample (~10 mg) was heated inside the extrusion device. After slow cooling, the fiber was extruded in the liquid crystal phase, and cooled to 23 °C. Typically, the aligned samples have a thickness of 0.3–0.7 mm and a length of 3–7 mm. All XRD measurements were done with the aligned sample axis perpendicular to the beam direction. Primary XRD analysis was performed using Datasqueeze (version 3.0.5).[83–87]

Molecular modelling, simulation, and electron density maps

Molecular models were drawn using DS ViewerPro (version 5.0) software. Material Studio Modeling (version 3.1) software from Accelrys was used to perform the energy minimizations of the built models on the supramolecular structures. BIOVIA Discovery Studio Visualizer (version 2019) was used for display style and coloring. Color codes were discussed in the caption of the Figures. Details were reported previously.[2,76–80] The electron density maps were reconstructed *via* principles previously employed for the supramolecular columns self-organized in the Φ_h phases and the procedure was detailed in our publications.[2,7,12]

Author contributions

Virgil Percec: conceptualization, data analysis, supervision and funding acquisition, investigation, and writing – original draft; Dipankar Sahoo: methodology, data analysis, graphics design; writing – review and editing, Mihai Peterca: data analysis; Mohammad R. Imam: synthesis, methodology; Devendra Maurya: synthesis, methodology, writing – review and editing.

12276 | *J. Mater. Chem. B*, 2024, **12**, 12265–12281

This journal is © The Royal Society of Chemistry 2024

Data availability

The data supporting this article are in the text of the manuscript.

Conflicts of interest

The authors declare that they have no competing interests.

Acknowledgements

References

1 P. Agre, Aquaporin Water Channels (Nobel Lecture), *Angew. Chem., Int. Ed.*, 2004, **43**, 4278–4290.

2 V. Percec, A. E. Dulcey, V. S. K. Balagurusamy, Y. Miura, J. Smidrkal, M. Peterca, S. Nummelin, U. Edlund, S. D. Hudson, P. A. Heiney, H. Duan, S. N. Magonov and S. A. Vinogradov, Self-assembly of amphiphilic dendritic dipeptides into helical pores, *Nature*, 2004, **430**, 764–768.

3 V. Percec, A. E. Dulcey, M. Peterca, M. Ilies, J. Ladislaw, B. M. Rosen, U. Edlund and P. A. Heiney, The Internal Structure of Helical Pores Self-Assembled from Dendritic Dipeptides is Stereochemically Programmed and Allosterically Regulated, *Angew. Chem., Int. Ed.*, 2005, **44**, 6516–6521.

4 V. Percec, A. E. Dulcey, M. Peterca, M. Ilies, M. J. Sienkowska and P. A. Heiney, Programming the Internal Structure and Stability of Helical Pores Self-Assembled from Dendritic Dipeptides via the Protective Groups of the Peptide, *J. Am. Chem. Soc.*, 2005, **127**, 17902–17909.

5 V. Percec, A. Dulcey, M. Peterca, M. Ilies, Y. Miura, U. Edlund and P. A. Heiney, Helical Porous Protein Mimics Self-Assembled from Amphiphilic Dendritic Dipeptides, *Aust. J. Chem.*, 2005, **58**, 472–482.

6 V. Percec, A. E. Dulcey, M. Peterca, M. Ilies, S. Nummelin, M. J. Sienkowska and P. A. Heiney, Principles of self-assembly of helical pores from dendritic dipeptides, *Proc. Natl. Acad. Sci. U. S. A.*, 2006, **103**, 2518–2523.

7 M. Peterca, V. Percec, A. E. Dulcey, S. Nummelin, S. Korey, M. Ilies and P. A. Heiney, Self-Assembly, Structural, and Retrostructural Analysis of Dendritic Dipeptide Pores Undergoing Reversible Circular to Elliptical Shape Change, *J. Am. Chem. Soc.*, 2006, **128**, 6713–6720.

8 V. Percec, A. E. Dulcey, M. Peterca, P. Adelman, R. Samant, V. S. K. Balagurusamy and P. A. Heiney, Helical Pores Self-Assembled from Homochiral Dendritic Dipeptides Based on L-Tyr and Nonpolar α-Amino Acids, *J. Am. Chem. Soc.*, 2007, **129**, 5992–6002.

9 M. S. Kaucher, M. Peterca, A. E. Dulcey, A. J. Kim, S. A. Vinogradov, D. A. Hammer, P. A. Heiney and V. Percec, Selective Transport of Water Mediated by Porous Dendritic Dipeptides, *J. Am. Chem. Soc.*, 2007, **129**, 11698–11699.

10 A. J. Kim, M. S. Kaucher, K. P. Davis, M. Peterca, M. R. Imam, N. A. Christian, D. H. Levine, F. S. Bates, V. Percec and D. A. Hammer, Proton Transport from Dendritic Helical-Pore-Incorporated Polymersomes, *Adv. Funct. Mater.*, 2009, **19**, 2930–2936.

11 B. M. Rosen, M. Peterca, K. Morimitsu, A. E. Dulcey, P. Leowanawat, A.-M. Resmerita, M. R. Imam and V. Percec, Programming the Supramolecular Helical Polymerization of Dendritic Dipeptides via the Stereochemical Information of the Dipeptide, *J. Am. Chem. Soc.*, 2011, **133**, 5135–5151.

12 V. Percec, M. Peterca, A. E. Dulcey, M. R. Imam, S. D. Hudson, S. Nummelin, P. Adelman and P. A. Heiney, Hollow Spherical Supramolecular Dendrimers, *J. Am. Chem. Soc.*, 2008, **130**, 13079–13094.

13 Y. Itoh, S. Chen, R. Hirahara, T. Konda, T. Aoki, T. Ueda, I. Shimada, J. J. Cannon, C. Shao, J. Shiomi, K. V. Tabata, H. Noji, K. Sato and T. Aida, Ultrafast water permeation through nanochannels with a densely fluorous interior surface, *Science*, 2022, **376**, 738–743.

14 I. M. Andrei, A. Chaix, B. T. Benkhaled, R. Dupuis, C. Gomri, E. Petit, M. Polentarutti, A. Van Der Lee, M. Semsarilar and M. Barboiu, Selective Water Pore Recognition and Transport through Self-Assembled Alkyl-Ureido-Trianglamine Artificial Water Channels, *J. Am. Chem. Soc.*, 2023, **145**, 21213–21221.

15 D.-D. Su and M. Barboiu, Hydrogen-bonded water-wires/clusters −Toward natural selectivity of artificial water channels, *Coord. Chem. Rev.*, 2024, **515**, 215973.

16 Y. J. Lim, K. Goh and R. Wang, The coming of age of water channels for separation membranes: from biological to biomimetic to synthetic, *Chem. Soc. Rev.*, 2022, **51**, 4537–4582.

17 D. Su, S. Ulrich and M. Barboiu, Bis-Alkylureido Imidazole Artificial Water Channels, *Angew. Chem., Int. Ed.*, 2023, **62**, e202306265.

18 C. Dutta, P. Krishnamurthy, D. Su, S. H. Yoo, G. W. Collie, M. Pasco, J. K. Marzinek, P. J. Bond, C. Verma, A. Grélard, A. Loquet, J. Li, M. Luo, M. Barboiu, G. Guichard, R. M. Kini and P. P. Kumar, Nature-inspired synthetic oligourea foldamer channels allow water transport with high salt rejection, *Chem*, 2023, **9**, 2237–2254.

19 D.-D. Su and M. Barboiu, Artificial Water Channels—Progress Innovations and Prospects, *CCS Chem.*, 2023, **5**, 279–291.

20 D.-D. Su and M. Barboiu, Hydrogen-bonded water-wires/clusters −Toward natural selectivity of artificial water channels, *Coord. Chem. Rev.*, 2024, **515**, 215973.

21 V. Percec, W.-D. Cho, G. Ungar and D. J. P. Yeardley, Synthesis and Structural Analysis of Two Constitutional Isomeric Libraries of AB₂-Based Monodendrons and
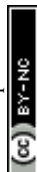
This journal is © The Royal Society of Chemistry 2024

J. Mater. Chem. B, 2024, **12**, 12265–12281 | **12277**

Supramolecular Dendrimers, *J. Am. Chem. Soc.*, 2001, **123**, 1302–1315.

22 V. Percec, C. M. Mitchell, W.-D. Cho, S. Uchida, M. Glodde, G. Ungar, X. Zeng, Y. Liu, V. S. K. Balagurusamy and P. A. Heiney, Designing Libraries of First Generation AB$_3$ and AB$_2$ Self-Assembling Dendrons via the Primary Structure Generated from Combinations of (AB)$_y$–AB$_3$ and (AB)$_y$–AB$_2$ Building Blocks, *J. Am. Chem. Soc.*, 2004, **126**, 6078–6094.

23 V. Percec, M. N. Holerca, S. Nummelin, J. J. Morrison, M. Glodde, J. Smidrkal, M. Peterca, B. M. Rosen, S. Uchida, V. S. K. Balagurusamy, M. J. Sienkowska and P. A. Heiney, Exploring and Expanding the Structural Diversity of Self-Assembling Dendrons through Combinations of AB, Constitutional Isomeric AB$_2$, and AB$_3$ Biphenyl-4-Methyl Ether Building Blocks, *Chem. – Eur. J.*, 2006, **12**, 6216–6241.

24 V. Percec, M. Peterca, M. J. Sienkowska, M. A. Ilies, E. Aqad, J. Smidrkal and P. A. Heiney, Synthesis and Retrostructural Analysis of Libraries of AB$_3$ and Constitutional Isomeric AB$_2$ Phenylpropyl Ether-Based Supramolecular Dendrimers, *J. Am. Chem. Soc.*, 2006, **128**, 3324–3334.

25 V. Percec, B. C. Won, M. Peterca and P. A. Heiney, Expanding the Structural Diversity of Self-Assembling Dendrons and Supramolecular Dendrimers via Complex Building Blocks, *J. Am. Chem. Soc.*, 2007, **129**, 11265–11278.

26 B. M. Rosen, D. A. Wilson, C. J. Wilson, M. Peterca, B. C. Won, C. Huang, L. R. Lipski, X. Zeng, G. Ungar, P. A. Heiney and V. Percec, Predicting the Structure of Supramolecular Dendrimers via the Analysis of Libraries of AB$_3$ and Constitutional Isomeric AB$_2$ Biphenylpropyl Ether Self-Assembling Dendrons, *J. Am. Chem. Soc.*, 2009, **131**, 17500–17521.

27 V. Percec, S. Wang, N. Huang, B. E. Partridge, X. Wang, D. Sahoo, D. J. Hoffman, J. Malineni, M. Peterca, R. L. Jezorek, N. Zhang, H. Daud, P. D. Sung, E. R. McClure and S. L. Song, An Accelerated Modular-Orthogonal Ni-Catalyzed Methodology to Symmetric and Nonsymmetric Constitutional Isomeric AB$_2$ to AB$_9$ Dendrons Exhibiting Unprecedented Self-Organizing Principles, *J. Am. Chem. Soc.*, 2021, **143**, 17724–17743.

28 D. A. Tomalia and S. N. Khanna, A Systematic Framework and Nanoperiodic Concept for Unifying Nanoscience: Hard/Soft Nanoelements, Superatoms, Meta-Atoms, New Emerging Properties, Periodic Property Patterns, and Predictive Mendeleev-like Nanoperiodic Tables, *Chem. Rev.*, 2016, **116**, 2705–2774.

29 V. Percec, J. Smidrkal, M. Peterca, C. M. Mitchell, S. Nummelin, A. E. Dulcey, M. J. Sienkowska and P. A. Heiney, Self-Assembly of Hybrid Dendrons with Complex Primary Structure Into Functional Helical Pores, *Chem. – Eur. J.*, 2007, **13**, 3989–4007.

30 V. Percec, D. Schlueter, Y. K. Kwon, J. Blackwell, M. Moeller and P. J. Slangen, Dramatic Stabilization of a Hexagonal Columnar Mesophase Generated from Supramolecular and Macromolecular Columns by the Semifluorination of the Alkyl Groups of Their Tapered Building Blocks, *Macromolecules*, 1995, **28**, 8807–8818.

31 G. Johansson, V. Percec, G. Ungar and J. P. Zhou, Fluorophobic Effect in the Self-Assembly of Polymers and Model Compounds Containing Tapered Groups into Supramolecular Columns, *Macromolecules*, 1996, **29**, 646–660.

32 G. Johansson, V. Percec, G. Ungar and K. Smith, Fluorophobic Effect Generates a Systematic Approach to the Synthesis of the Simplest Class of Rodlike Liquid Crystals Containing a Single Benzene Unit, *Chem. Mater.*, 1997, **9**, 164–175.

33 V. Percec, G. Johansson, G. Ungar and J. Zhou, Fluorophobic Effect Induces the Self-Assembly of Semifluorinated Tapered Monodendrons Containing Crown Ethers into Supramolecular Columnar Dendrimers Which Exhibit a Homeotropic Hexagonal Columnar Liquid Crystalline Phase, *J. Am. Chem. Soc.*, 1996, **118**, 9855–9866.

34 S. D. Hudson, H.-T. Jung, V. Percec, W.-D. Cho, G. Johansson, G. Ungar and V. S. K. Balagurusamy, Direct Visualization of Individual Cylindrical and Spherical Supramolecular Dendrimers, *Science*, 1997, **278**, 449–452.

35 V. Percec, D. Schlueter and G. Ungar, Rational Design of a Hexagonal Columnar Mesophase in Telechelic Alternating Multicomponent Semifluorinated Polyethylene Oligomers, *Macromolecules*, 1997, **30**, 645–648.

36 V. Percec, M. Glodde, T. K. Bera, Y. Miura, I. Shiyanovskaya, K. D. Singer, V. S. K. Balagurusamy, P. A. Heiney, I. Schnell, A. Rapp, H.-W. Spiess, S. D. Hudson and H. Duan, Self-organization of supramolecular helical dendrimers into complex electronic materials, *Nature*, 2002, **419**, 384–387.

37 V. Percec and T. K. Bera, Cell membrane as a model for the design of semifluorinated ion-selective nanostructured supramolecular systems, *Tetrahedron*, 2002, **58**, 4031–4040.

38 D. R. Dukeson, G. Ungar, V. S. K. Balagurusamy, V. Percec, G. A. Johansson and M. Glodde, Application of Isomorphous Replacement in the Structure Determination of a Cubic Liquid Crystal Phase and Location of Counterions, *J. Am. Chem. Soc.*, 2003, **125**, 15974–15980.

39 V. Percec, M. Glodde, G. Johansson, V. S. K. Balagurusamy and P. A. Heiney, Transformation of a Spherical Supramolecular Dendrimer into a Pyramidal Columnar Supramolecular Dendrimer Mediated by the Fluorophobic Effect, *Angew. Chem., Int. Ed.*, 2003, **42**, 4338–4342.

40 V. Percec, M. R. Imam, T. K. Bera, V. S. K. Balagurusamy, M. Peterca and P. A. Heiney, Self-Assembly of Semifluorinated Janus-Dendritic Benzamides into Bilayered Pyramidal Columns, *Angew. Chem., Int. Ed.*, 2005, **44**, 4739–4745.

41 Y.-C. Wu, P. Leowanawat, H.-J. Sun, B. E. Partridge, M. Peterca, R. Graf, H. W. Spiess, X. Zeng, G. Ungar, C.-S. Hsu, P. A. Heiney and V. Percec, Complex Columnar Hexagonal Polymorphism in Supramolecular Assemblies of a Semifluorinated Electron-Accepting Naphthalene Bisimide, *J. Am. Chem. Soc.*, 2015, **137**, 807–819.

42 M.-S. Ho, B. E. Partridge, H.-J. Sun, D. Sahoo, P. Leowanawat, M. Peterca, R. Graf, H. W. Spiess, X. Zeng, G. Ungar, P. A. Heiney, C.-S. Hsu and V. Percec, Screening Libraries of Semifluorinated Arylene Bisimides

12278 | *J. Mater. Chem. B*, 2024, **12**, 12265–12281

This journal is © The Royal Society of Chemistry 2024

to Discover and Predict Thermodynamically Controlled Helical Crystallization, *ACS Comb. Sci.*, 2016, **18**, 723–739.

43 V. Percec, M. Glodde, M. Peterca, A. Rapp, I. Schnell, H. W. Spiess, T. K. Bera, Y. Miura, V. S. K. Balagurusamy, E. Aqad and P. A. Heiney, Self-Assembly of Semifluorinated Dendrons Attached to Electron-Donor Groups Mediates Their π-Stacking via a Helical Pyramidal Column, *Chem. – Eur. J.*, 2006, **12**, 6298–6314.

44 V. Percec, E. Aqad, M. Peterca, M. R. Imam, M. Glodde, T. K. Bera, Y. Miura, V. S. K. Balagurusamy, P. C. Ewbank, F. Würthner and P. A. Heiney, Self-Assembly of Semifluorinated Minidendrons Attached to Electron-Acceptor Groups into Pyramidal Columns, *Chem. – Eur. J.*, 2007, **13**, 3330–3345.

45 V. Percec and M. Lee, Molecular Engineering of Liquid Crystal Polymers by Living Polymerization. XXIII. Synthesis and Characterization of AB Block Copolymers Based on ω-[(4-Cyano-4′-Biphenyl)-oxy]alkyl Vinyl Ether, 1*H*,1*H*,2*H*,2*H*-Perfluorodecyl Vinyl Ether, and 2-(4-Blphenyloxy)ethyl Vinyl Ether with 1*H*,1*H*,2*H*,2*H*-Perfluorodecyl Vinyl Ether, *J. Macromol. Sci., Part A: Pure Appl. Chem.*, 1992, **29**, 723–740.

46 Q. Xiao, J. D. Rubien, Z. Wang, E. H. Reed, D. A. Hammer, D. Sahoo, P. A. Heiney, S. S. Yadavalli, M. Goulian, S. E. Wilner, T. Baumgart, S. A. Vinogradov, M. L. Klein and V. Percec, Self-Sorting and Coassembly of Fluorinated, Hydrogenated, and Hybrid Janus Dendrimers into Dendrimersomes, *J. Am. Chem. Soc.*, 2016, **138**, 12655–12663.

47 Q. Xiao, S. E. Sherman, S. E. Wilner, X. Zhou, C. Dazen, T. Baumgart, E. H. Reed, D. A. Hammer, W. Shinoda, M. L. Klein and V. Percec, Janus dendrimersomes coassembled from fluorinated, hydrogenated, and hybrid Janus dendrimers as models for cell fusion and fission, *Proc. Natl. Acad. Sci. U. S. A.*, 2017, **114**, E7045–E7053.

48 P. Torre, Q. Xiao, I. Buzzacchera, S. E. Sherman, K. Rahimi, N. Y. Kostina, C. Rodriguez-Emmenegger, M. Möller, C. J. Wilson, M. L. Klein, M. C. Good and V. Percec, Encapsulation of hydrophobic components in dendrimersomes and decoration of their surface with proteins and nucleic acids, *Proc. Natl. Acad. Sci. U. S. A.*, 2019, **116**, 15378–15385.

49 S. E. Wilner, Q. Xiao, Z. T. Graber, S. E. Sherman, V. Percec and T. Baumgart, Dendrimersomes Exhibit Lamellar-to-Sponge Phase Transitions, *Langmuir*, 2018, **34**, 5527–5534.

50 V. Percec, M. R. Imam, M. Peterca and P. Leowanawat, Self-organizable vesicular columns assembled from polymers dendronized with semifluorinated janus dendrimers act as reverse thermal actuators, *J. Am. Chem. Soc.*, 2012, **134**, 4408–4420.

51 C. J. Wilson, D. A. Wilson, A. E. Feiring and V. Percec, Disassembly via an environmentally friendly and efficient fluorous phase constructed with dendritic architectures, *J. Polym. Sci., Part A: Polym. Chem.*, 2010, **48**, 2498–2508.

52 M. Peterca, M. R. Imam, A. E. Dulcey, K. Morimitsu, Q. Xiao, D. S. Maurya and V. Percec, Molecular parameters including fluorination program order during hierarchical

helical self-organization of self-assembling dendrons, *Giant*, 2022, **11**, 100103.

53 I. T. Horváth and J. Rábai, Facile Catalyst Separation Without Water: Fluorous Biphase Hydroformylation of Olefins, *Science*, 1994, **266**, 72–75.

54 J. A. Gladysz, D. P. Curran and T. T. Horvath, *Handbook of Fluorous Chemistry*, Wiley-VCH, Weinheim, 1., Auflage, neue Ausg., 2006.

55 W. Zhang and D. P. Curran, Synthetic applications of fluorous solid-phase extraction (F-SPE), *Tetrahedron*, 2006, **62**, 11837–11865.

56 A. P. Dobbs and M. R. Kimberley, Fluorous phase chemistry: a new industrial technology, *J. Fluorine Chem.*, 2002, **118**, 3–17.

57 W. Zhang, Fluorous tagging strategy for solution-phase synthesis of small molecules, peptides and oligosaccharides, *Curr. Opin. Drug. Discovery Dev.*, 2004, **7**, 784–797.

58 M. P. Krafft, Controlling phospholipid self-assembly and film properties using highly fluorinated components – Fluorinated monolayers, vesicles, emulsions and microbubbles, *Biochimie*, 2012, **94**, 11–25.

59 M. Rosati, A. Acocella, A. Pizzi, G. Turtù, G. Neri, N. Demitri, Nonappa, G. Raffaini, B. Donnio, F. Zerbetto, F. B. Bombelli, G. Cavallo and P. Metrangolo, Janus-Type Dendrimers Based on Highly Branched Fluorinated Chains with Tunable Self-Assembly and ^{19}F Nuclear Magnetic Resonance Properties, *Macromolecules*, 2022, **55**, 2486–2496.

60 J.-M. Vincent, Recent advances of fluorous chemistry in material sciences, *Chem. Commun.*, 2012, **48**, 11382.

61 M. Guerre, G. Lopez, B. Améduri, M. Semsarilar and V. Ladmiral, Solution self-assembly of fluorinated polymers, an overview, *Polym. Chem.*, 2021, **12**, 3852–3877.

62 M. H. C. J. Van Houtem, F. Benaskar, C. F. C. Fitié, R. Martín-Rapún, J. A. J. M. Vekemans and E. W. Meijer, Helical self-assembly and co-assembly of fluorinated, preorganized discotics, *Org. Biomol. Chem.*, 2012, **10**, 5898.

63 C. Tschierske, *Topics in Current Chemistry. Liquid Crystals. Material Design and Self-Assembly*, Springer, 2012.

64 H.-J. Sun, S. Zhang and V. Percec, From structure to function via complex supramolecular dendrimer systems, *Chem. Soc. Rev.*, 2015, **44**, 3900–3923.

65 M.-D. Zhang, J.-R. Huang, W. Shi, P.-Q. Liao and X.-M. Chen, Synergistic Effect in a Metal–Organic Framework Boosting the Electrochemical CO_2 Overall Splitting, *J. Am. Chem. Soc.*, 2023, **145**, 2439–2447.

66 W. Fan, B. Yung, P. Huang and X. Chen, Nanotechnology for Multimodal Synergistic Cancer Therapy, *Chem. Rev.*, 2017, **117**, 13566–13638.

67 S. Gao, L. Wang, C. Zhao, A. Wang, X. Lang, Z. Liu and W. Wang, A review of the synergistic effect of multi-coordination crystal fields on electrocatalysts, *Mater. Chem. Front.*, 2021, **5**, 6718–6734.

68 Q. Yang, Q. Xu and H.-L. Jiang, Metal–organic frameworks meet metal nanoparticles: synergistic effect for enhanced catalysis, *Chem. Soc. Rev.*, 2017, **46**, 4774–4808.

This journal is © The Royal Society of Chemistry 2024

J. Mater. Chem. B, 2024, **12**, 12265–12281 | **12279**

69 Y. Deng, S. Kumar and H. Wang, Synergistic–cooperative combination of enamine catalysis with transition metal catalysis, *Chem. Commun.*, 2014, **50**, 4272–4284.

70 R. W. Saalfrank, H. Maid and A. Scheurer, Supramolecular Coordination Chemistry: The Synergistic Effect of Serendipity and Rational Design, *Angew. Chem., Int. Ed.*, 2008, **47**, 8794–8824.

71 T. Chen, M. Qiu, Y. Peng, C. Yi and Z. Xu, Engineering synergistic effects of immobilized cooperative catalysts, *Coord. Chem. Rev.*, 2023, **474**, 214863.

72 X. Jiang, S. Fleischmann, N. H. Nguyen, B. M. Rosen and V. Percec, Cooperative and synergistic solvent effects in SET-LRP of MA, *J. Polym. Sci., Part A: Polym. Chem.*, 2009, **47**, 5591–5605.

73 D. S. Maurya, J. Adamson, N. Bensabeh, G. Lligadas and V. Percec, Catalytic effect of DMSO in metal-catalyzed radical polymerization mediated by disproportionation facilitates living and immortal radical polymerizations, *J. Polym. Sci.*, 2023, **61**, 959–978.

74 N. H. Nguyen, M. E. Levere and V. Percec, SET-LRP of methyl acrylate to complete conversion with zero termination, *J. Polym. Sci., Part A: Polym. Chem.*, 2012, **50**, 860–873.

75 V. Percec, C. Grigoras and H.-J. Kim, Toward self-assembling dendritic macromolecules from conventional monomers by a combination of living radical polymerization and irreversible terminator multifunctional initiator, *J. Polym. Sci., Part A: Polym. Chem.*, 2004, **42**, 505–513.

76 V. Percec, T. K. Bera, M. Glodde, Q. Fu, V. S. K. Balagurusamy and P. A. Heiney, Hierarchical Self-Assembly, Coassembly, and Self-Organization of Novel Liquid Crystalline Lattices and Superlattices from a Twin-Tapered Dendritic Benzamide and Its Four-Cylinder-Bundle Supramolecular Polymer, *Chem. – Eur. J.*, 2003, **9**, 921–935.

77 V. Percec, M. Peterca, T. Tadjiev, X. Zeng, G. Ungar, P. Leowanawat, E. Aqad, M. R. Imam, B. M. Rosen, U. Akbey, R. Graf, S. Sekharan, D. Sebastiani, H. W. Spiess, P. A. Heiney and S. D. Hudson, Self-Assembly of Dendronized Perylene Bisimides into Complex Helical Columns, *J. Am. Chem. Soc.*, 2011, **133**, 12197–12219.

78 V. Percec and A. Keller, A thermodynamic interpretation of polymer molecular weight effect on the phase transitions of main-chain and side-chain liquid-crystal polymers, *Macromolecules*, 1990, **23**, 4347–4350.

79 V. Percec and D. Tomazos, Recent Developments in Tailor-Made Liquid Crystalline Polymers, *Indian J. Technol.*, 1993, **31**, 339–392.

80 D. Sahoo, M. Peterca and V. Percec, Designing Highly Ordered Helical and Nonhelical Porous Crystalline and Disordered Nonhelical Columnar Liquid Crystalline Self-Organizations, *J. Am. Chem. Soc.*, 2024, **146**, 22943–22949.

81 D. Sahoo, M. Peterca and V. Percec, Hierarchical Self-Organization and Disorganization of Helical Supramolecular Columns Mediated by H-Bonding and Shape Complementarity, *J. Am. Chem. Soc.*, 2024, **146**, 27299–27304.

82 D. Sahoo, M. Peterca, P. Leowanawat and V. Percec, Cogwheel Mechanism of Helical Self-Organization is Thermodynamically Controlled, Self-Repairing, and Universal, *J. Am. Chem. Soc.*, 2024, **146**, 18910–18915.

83 P. A. Heiney, Commission on Powder Diffraction Newsletter, *IUCr Conference*, 2005, vol. 32, pp. 9–11.

84 V. Percec, H.-J. Sun, P. Leowanawat, M. Peterca, R. Graf, H. W. Spiess, X. Zeng, G. Ungar and P. A. Heiney, Transformation from Kinetically into Thermodynamically Controlled Self-Organization of Complex Helical Columns with 3D Periodicity Assembled from Dendronized Perylene Bisimides, *J. Am. Chem. Soc.*, 2013, **135**, 4129–4148.

85 B. M. Rosen, C. J. Wilson, D. A. Wilson, M. Peterca, M. R. Imam and V. Percec, Dendron-Mediated Self-Assembly, Disassembly, and Self-Organization of Complex Systems, *Chem. Rev.*, 2009, **109**, 6275–6540.

86 M. Peterca, V. Percec, M. R. Imam, P. Leowanawat, K. Morimitsu and P. A. Heiney, Molecular Structure of Helical Supramolecular Dendrimers, *J. Am. Chem. Soc.*, 2008, **130**, 14840–14852.

87 D. Sahoo, E. Aqad, M. Peterca and V. Percec, Molecular design principles of helical pyramidal chirality self-organized from achiral hexakis(alkyloxy)triphenylene, *Giant*, 2023, **13**, 100138.

88 C. W. Bunn and E. R. Howells, Structures of Molecules and Crystals of Fluoro-Carbons, *Nature*, 1954, **174**, 549–551.

89 K. Monde, N. Miura, M. Hashimoto, T. Taniguchi and T. Inabe, Conformational Analysis of Chiral Helical Perfluoroalkyl Chains by VCD, *J. Am. Chem. Soc.*, 2006, **128**, 6000–6001.

90 K. Ute, R. Kinoshita, K. Matsui, N. Miyatake and K. Hatada, Conformational Asymmetry of a Linear Perfluoroalkyl Chain in Solution. Dynamic Fluorine-19 NMR Spectroscopy of the Perfluoro-*n*-alkanes Carrying a Chiral End-Group as a Probe of Magnetic Nonequivalence, *Chem. Lett.*, 1992, 1337–1340.

91 N. Terasawa, H. Monobe, K. Kiyohara and Y. Shimizu, Strong tendency towards homeotropic alignment in a hexagonal columnar mesophase of fluoroalkylated triphenylenes, *Chem. Commun.*, 2003, 1678.

92 D. K. Yoon, S. R. Lee, Y. H. Kim, S.-M. Choi and H.-T. Jung, Large-Area, Highly Aligned Cylindrical Perfluorinated Supramolecular Dendrimers Using Magnetic Fields, *Adv. Mater.*, 2006, **18**, 509–513.

93 L. Huang, M. Di Vincenzo, Y. Li and M. Barboiu, Artificial Water Channels: Towards Biomimetic Membranes for Desalination, *Chem. – Eur. J.*, 2021, **27**, 2224–2239.

94 W. Song, C. Lang, Y. Shen and M. Kumar, Design Considerations for Artificial Water Channel–Based Membranes, *Annu. Rev. Mater. Res.*, 2018, **48**, 57–82.

95 W. Song and M. Kumar, Artificial water channels: toward and beyond desalination, *Curr. Opin. Chem. Eng.*, 2019, **25**, 9–17.

96 T. Jiang, A. Hall, M. Eres, Z. Hemmatian, B. Qiao, Y. Zhou, Z. Ruan, A. D. Couse, W. T. Heller, H. Huang, M. O. De La Cruz, M. Rolandi and T. Xu, Single-chain heteropolymers

12280 | *J. Mater. Chem. B*, 2024, **12**, 12265–12281

This journal is © The Royal Society of Chemistry 2024

transport protons selectively and rapidly, *Nature*, 2020, **577**, 216–220.

97 Y. Chen, H.-Y. Chang, M.-T. Lee, Z.-R. Yang, C.-H. Wang, K.-Y. Wu, W.-T. Chuang and C.-L. Wang, Dual-Axis Alignment of Bulk Artificial Water Channels by Directional Water-Induced Self-Assembly, *J. Am. Chem. Soc.*, 2022, **144**, 7768–7777.

98 J. Shen, A. Roy, H. Joshi, L. Samineni, R. Ye, Y.-M. Tu, W. Song, M. Skiles, M. Kumar, A. Aksimentiev and H. Zeng, Fluorofoldamer-Based Salt- and Proton-Rejecting Artificial Water Channels for Ultrafast Water Transport, *Nano Lett.*, 2022, **22**, 4831–4838.

99 A. Roy, J. Shen, H. Joshi, W. Song, Y.-M. Tu, R. Chowdhury, R. Ye, N. Li, C. Ren, M. Kumar, A. Aksimentiev and H. Zeng, Foldamer-based ultrapermeable and highly selective artificial water channels that exclude protons, *Nat. Nanotechnol.*, 2021, **16**, 911–917.

100 Y. Shen, W. Si, M. Erbakan, K. Decker, R. De Zorzi, P. O. Saboe, Y. J. Kang, S. Majd, P. J. Butler, T. Walz, A. Aksimentiev, J. Hou and M. Kumar, Highly permeable artificial water channels that can self-assemble into two-dimensional arrays, *Proc. Natl. Acad. Sci. U. S. A.*, 2015, **112**, 9810–9815.

101 N. C. Yoder and K. Kumar, Fluorinated amino acids in protein design and engineering, *Chem. Soc. Rev.*, 2002, **31**, 335–341.

102 M. Salwiczek, E. K. Nyakatura, U. I. M. Gerling, S. Ye and B. Koksch, Fluorinated amino acids: compatibility with native protein structures and effects on protein–protein interactions, *Chem. Soc. Rev.*, 2012, **41**, 2135–2171.

103 D. R. Coulson, L. C. Satek and S. O. Grim, in *Inorganic Syntheses*, ed. F. A. Cotton, Wiley, 1st edn, 1972, vol. 13, pp. 121–124.

104 G. Ungar, D. Abramic, V. Percec and J. A. Heck, Self-Assembly of Twin Tapered Bismides into Supramolecular Columns Exhibittng Hexagonal Columnar Mesophases. Structural Evidence for a Microsegregated Model of the Supramolecular Column, *Liq. Cryst.*, 1996, **21**, 73–86.

105 N. Zhang, S. R. Samanta, B. M. Rosen and V. Percec, Single Electron Transfer in Radical Ion and Radical-Mediated Organic, Materials and Polymer Synthesis, *Chem. Rev.*, 2014, **114**, 5848–5958.

106 B. M. Rosen and V. Percec, Single-Electron Transfer and Single-Electron Transfer Degenerative Chain Transfer Living Radical Polymerization, *Chem. Rev.*, 2009, **109**, 5069–5119.

107 S. R. Samanta, M. E. Levere and V. Percec, SET-LRP of hydrophobic and hydrophilic acrylates in trifluoroethanol, *Polym. Chem.*, 2013, **4**, 3212–3224.

108 S. R. Samanta, A. Anastasaki, C. Waldron, D. M. Haddleton and V. Percec, SET-LRP of methacrylates in fluorinated alcohols, *Polym. Chem.*, 2013, **4**, 5563–5569.

109 S. R. Samanta, A. Anastasaki, C. Waldron, D. M. Haddleton and V. Percec, SET-LRP of hydrophobic and hydrophilic acrylates in tetrafluoropropanol, *Polym. Chem.*, 2013, **4**, 5555–5562.

110 S. R. Samanta, R. Cai and V. Percec, SET-LRP of semi-fluorinated acrylates and methacrylates, *Polym. Chem.*, 2014, **5**, 5479–5491.

111 S. R. Samanta and V. Percec, Synthesis of high molar mass poly(*n*-butyl acrylate) and poly(2-ethylhexyl acrylate) by SET-LRP in mixtures of fluorinated alcohols with DMSO, *Polym. Chem.*, 2014, **5**, 169–174.

112 S. R. Samanta, H.-J. Sun, A. Anastasaki, D. M. Haddleton and V. Percec, Self-activation and activation of Cu(0) wire for SET-LRP mediated by fluorinated alcohols, *Polym. Chem.*, 2014, **5**, 89–95.

113 S. R. Samanta, R. Cai and V. Percec, A rational approach to activated polyacrylates and polymethacrylates by using a combination of model reactions and SET–LRP of hexafluoroisopropyl acrylate and methacrylate, *Polym. Chem.*, 2015, **6**, 3259–3270.

114 S. R. Samanta, R. Cai and V. Percec, Synthesis of amphiphilic homopolymers with high chain end functionality by SET–LRP, *J. Polym. Sci., Part A: Polym. Chem.*, 2015, **53**, 294–303.

115 A. E. Feiring, E. R. Wonchoba, F. Davidson, V. Percec and B. Barboiu, Fluorocarbon-ended polymers: metal catalyzed radical and living radical polymerizations initiated by perfluoroalkylsulfonyl halides, *J. Polym. Sci., Part A: Polym. Chem.*, 2000, **38**, 3313–3335.

116 V. Percec, J. H. Wang, Y. Oishi and A. E. Feiring, Synthesis of aromatic polythers by Scholl reaction. IV. Homopolymerization and copolymerization of α,ω-bis[4-(1-napthoxy)phenylsulfonyl]perfluoroalkanes, *J. Polym. Sci., Part A: Polym. Chem.*, 1991, **29**, 965–976.

117 V. Percec, D. Tomazos and A. E. Feiring, Semifluorinated polymers: 1. Synthesis and characterization of side chain liquid crystalline polymers containing semifluorinated oligooxyethylene based flexible spacers, *Polymer*, 1991, **32**, 1897–1908.

118 R. Rodenhouse, V. Percec and A. E. Feiring, Liquid crystal polymers containing macroheterocyclic ligands. 4. Synthesis of mesomorphic polymers containing crown ethers by cationic cyclocopolymerization of 1,2-bis(2-ethenyloxyethoxy)benzene with mesogenic vinyl ethers, *J. Polym. Sci., Part C: Polym. Lett.*, 1990, **28**, 345–355.

119 V. Percec, D. Sahoo and D. Maurya, Bridging Organic, Molecular, Macromolecular, Supramolecular and Biological Sciences to Create Functions via Fluorine Chemistry and Fluorinated Reagents, *Giant*, 2023, **16**, 100193.

This journal is © The Royal Society of Chemistry 2024

J. Mater. Chem. B, 2024, **12**, 12265–12281 | **12281**